This is a non-peer-reviewed preprint submitted to EarthArXiv.

Review of deep learning for tree species identification from high-resolution remote sensing imagery

This is a non-peer-reviewed preprint submitted to EarthArXiv

Zhongyu Xia[1], Teja Kattenborn[2], Jan D. Wegner[3], Arthur Gessler[1,4], Verena C. Griess[1], Mirela Beloiu[1*]*

[1] Department of Environmental Systems Science, Institute of Terrestrial Ecosystems, ETH Zurich, 8092 Zurich, Switzerland

[2] Chair of Sensor-based Geoinformatics, University of Freiburg, 79106 Freiburg, Germany

[3] Department of Mathematical Modeling and Machine Learning, University of Zurich, Zurich, 8057, Switzerland

[4] Forest and Soil Ecology, Swiss Federal Institute for Forest, Snow and Landscape Research WSL, 8903 Birmensdorf, Switzerland

*Corresponding authors: Zhongyu Xia (zhongyu.xia@usys.ethz.ch) and Mirela Beloiu (mirela.beloiu@usys.ethz.ch)

This is a non-peer-reviewed preprint submitted to EarthArXiv.

Review of deep learning for tree species identification from high-resolution remote sensing imagery

Abstract

Tree species information is essential for monitoring forest composition, carbon storage, biodiversity, and resilience to environmental change, but remains largely available only at local scales. Centimeter-resolution remotely sensed imagery and deep learning are shifting species mapping from stands to individual tree crowns, yet the diversity of tree species, data, and methods has fragmented this rapidly growing field. Here, we provide a systematic review to assess progress and define research priorities for crown-level tree species identification based primarily on centimeter-resolution 2D imagery and deep learning. We synthesized 133 studies published between 2017 and 2025, representing 1,034 deep learning-based crown-level species identification tasks across diverse ecosystems, sensor types, and modeling approaches. We found strong geographic and taxonomic biases, with 83% of studies concentrated on temperate and subtropical forests. RGB was the dominant input (62% of tasks), followed by multispectral (10%) and hyperspectral imagery (9%), while 17% used multimodal data. Among controlled 2D–3D comparisons, 60% showed improved performance. Among computer vision tasks, patch-wise classification accounted for 41%, followed by semantic segmentation (29%), object detection (18%), and instance segmentation (13%). CNNs remained the predominant architecture (77%) but new transformer-based and hybrid architectures are emerging. Cross-site transferability remains the central challenge to closing geographic and taxonomic gaps, requiring representative open datasets and standardized evaluation across sites and sensors.

Keywords: Individual tree crowns; aerial imagery; centimeter-resolution; multimodal data fusion; model transferability

Highlights

133 studies and 1,034 crown-level tree species identification tasks were reviewed

83% of tree species identification studies are on temperate and subtropical forests

Multispectral and hyperspectral data improved performance over RGB in 82% of comparisons

CNNs still dominate (77%), but transformer-hybrid models are an emerging trend

Standardized data sharing and transferable models are the field's key gaps

1. Introduction

The composition and distribution of tree species is one of the most critical components of forest science. They provide essential information for ecological research and effective forest management, which are directly linked to forest biodiversity (Barbier et al., 2008), ecological and economic value of forests (Van Der Plas et al., 2018), forest succession dynamics (Taylor et al., 2009), and invasive species monitoring (Vaz et al., 2018). As global forests face escalating pressures from climate change and land-use alteration, accurate and timely species mapping is

increasingly demanded by researchers and forest managers to support evidence-based decision-making and sustainable resource management. Meeting this need requires tools capable of delivering detailed, repeatable, and scalable insights, which are scarcely attainable through traditional ground surveys.

Remote sensing imagery plays a vital role in forest species mapping. For decades, forest species mapping has relied primarily on medium-resolution satellite imagery, such as Landsat (30 m) and Sentinel-2 (10 m), which capture mixed spectral signals from multiple trees and therefore support dominant species discrimination mainly at the stand level (Fassnacht et al., 2016; Pu, 2021). Recent advances in sensor and platform technology have increased the availability of very-high-resolution RGB (red-green-blue) imagery (5 to 25 cm) from aircraft, UAVs (uncrewed aerial vehicles), and commercial satellites, enabling individual tree crowns to be spatially resolved and analyzed through their spectral, structural, and textural characteristics (Nagendra, 2001; Zheng et al., 2025). This finer spatial resolution allows species identity to be resolved directly at the scale of individual crowns or crown clusters, rather than inferred from the spectrally mixed, stand-level signals of coarser sensors, thereby revealing fine-scale patterns of species presence and distribution that medium-resolution imagery cannot capture (Blaschke et al., 2014; Mustafa and Habeeb, 2014). Besides low-cost RGB imagery, the increasing availability of multispectral, hyperspectral, and LiDAR data enables the fusion of complementary spectral, structural, and temporal information, offering new opportunities to improve tree species identification, yet their relative contributions remain poorly synthesized (Brandt et al., 2024). Achieving scalable and operational tree species mapping requires more transferable models (B.G. Weinstein et al., 2023), automated workflows (Hamedianfar et al., 2022), and standardized reference datasets (Lines et al., 2022). This, in turn, requires understanding how acquisition platforms, sensor types, spatial resolution, and data-fusion strategies influence model performance.

Tree species have traditionally been identified through field inventories, which remain the primary source of reference labels for remote sensing applications. Prior to the deep learning era, species classification from remote sensing imagery relied on conventional machine learning algorithms, such as support vector machines and random forests, applied to hand-crafted spectral, textural, and shape features (e.g., vegetation indices, gray-level co-occurrence texture measures, and crown shape descriptors) extracted through expert-defined rules. The emergence of deep learning-based computer vision around 2017 (Christin et al., 2019; Zhu et al., 2017) fundamentally changed this paradigm by automatically learning image features directly from aerial imagery, reducing reliance on manual data engineering and enabling more accurate and scalable recognition of complex crown patterns (Hamedianfar et al., 2022; Kattenborn et al., 2021; Zhao et al., 2023). Tree species identification at the crown level (hereafter “TSI”) using high-resolution aerial imagery and computer vision is an emerging research field, positioned at the intersection of forestry, remote sensing, and artificial intelligence.

Deep learning-based computer vision tasks, such as image classification, semantic segmentation, object detection, and instance segmentation, have been widely applied to tree detection, crown delineation, and species classification (Kattenborn et al., 2021). Crown-level species identification can therefore be achieved through different pipelines: object detection and instance

segmentation directly localize individual crowns, whereas image classification and semantic segmentation can be combined with pre- or post-processing steps for crown detection or delineation. Zhao et al. (2023) showed that methods based on CNNs (convolutional neural networks) have substantially improved crown detection and delineation, despite persistent challenges in dense forests and limited training data. More recently, Vision Transformers, foundation models, and multimodal learning frameworks have expanded these approaches through improved feature representation, transfer learning, and data fusion. However, it remains unclear how these methodological advances translate into improved tree species identification across different forest types, remote sensing platforms, sensor modalities, and computer vision tasks (Pu, 2021; Santos et al., 2019).

Here, we move beyond previous work by providing the first quantitative synthesis of how forest characteristics, remote sensing data, computer vision tasks, and deep learning methodologies jointly influence tree species identification. To do so, we compiled a database and conducted a meta-analysis based on 1,034 tree species identification tasks reported in 133 peer-reviewed studies published between 2017 and 2025. Throughout, we refer to aerial imagery broadly as high-resolution optical imagery acquired from satellite, crewed aircraft, and UAV platforms. While RGB imagery forms the core focus because of its widespread availability and operational relevance, we also evaluate multispectral, hyperspectral, LiDAR, and related modalities when combined with RGB through data fusion. Our analysis addresses three overarching questions: (1) Forest: what tree species have been identified across forest biomes or forest types? (2) Remote sensing data: how do imagery types, sensors, platforms, and data fusion influence model performance? (3) Deep learning: which deep learning approaches and models have been applied? Our results present the global landscape of TSI research, reveal persistent geographic and taxonomic biases, and define priorities for developing scalable, transferable, and operational tree species identification systems.

2. Materials and methods

2.1. Literature search and selection

We conducted exhaustive searches across Scopus, Web of Science, and IEEE Xplore. The search was limited to English-language, peer-reviewed articles and conference proceedings published between 1 January 2012 and 31 December 2025. The search string, applied to the title, abstract, and author keywords, was structured as follows: ("tree" OR "forest" OR "canopy" OR "crown") AND ("individual" OR "single" OR "delineat*" OR "detect*" OR "discriminat*" OR "segment*" OR "map*") AND ("species classification" OR "species identification" OR "species detection" OR "species recognition") AND ("deep learning" OR "neural network" OR "DL" OR "CNN" OR "convolutional networks" OR "automat*" OR "instance segmentation" OR "object detection" OR "semantic segmentation"). After removing duplicates, the initial results yielded 790 studies (Fig. 1).

Two rounds of screening process were implemented to identify eligible articles. First, studies not primarily focused on trees were excluded, such as studies targeting other vegetation types (e.g., crops or flowers). Studies that included shrubs alongside trees were retained, given the

morphological and ecological continuum between these growth forms and their frequent co-occurrence in the remote sensing literature. In the second round, five predefined inclusion criteria were applied, aligning with the core scope of this review: (1) the identification was performed at the crown level, with target objects consisting of individual trees or crown clusters representing a single species; (2) tree species or genus labels were explicitly identified; (3) remote sensing imagery (UAV-, aircraft-, or satellite-based) with a spatial resolution ≤ 2 m served as the *primary* model input, thereby excluding studies solely relying on non-imagery data (such as LiDAR and SAR); (4) a deep learning model was employed for the pipeline of detection, segmentation, or classification; and (5) valid accuracy evaluation metrics were explicitly reported. Although the initial search spanned 2012–2025, all studies meeting the full set of criteria were published between 2017 and 2025, yielding a final total of 133 studies included in the subsequent meta-analysis.

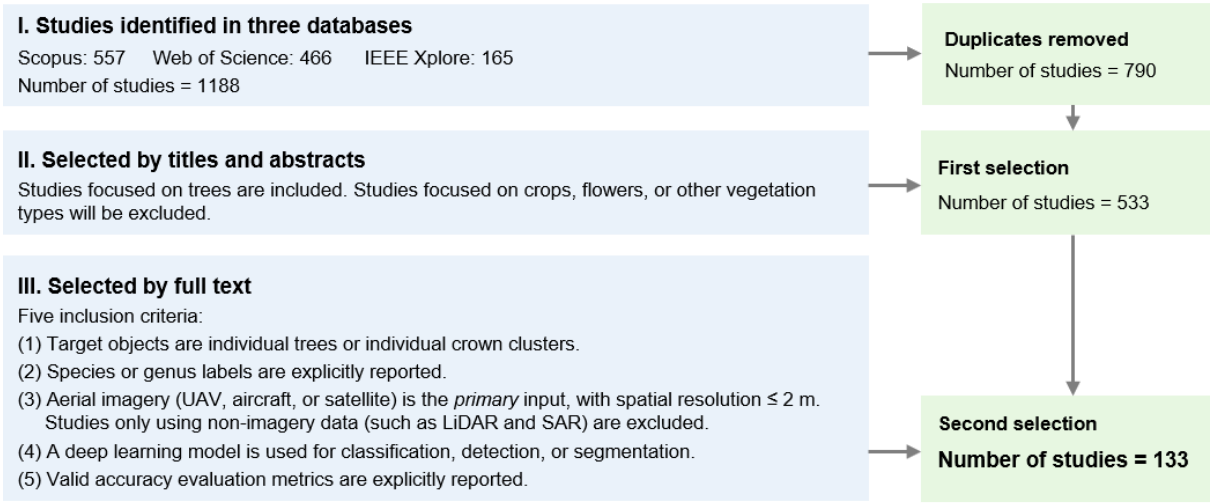


Fig. 1. PRISMA (Preferred Reporting Items for Systematic reviews and Meta-Analyses) flow diagram describing the selection phases (in blue) of this review and the final number of selected studies (in green).

2.2. Meta-data extraction and analysis

When constructing the meta-database, we extracted two levels of records from each article for use in different statistical analyses: *publication* and *identification task*. At the publication level, this study conducted multiple descriptive statistics to characterize the general patterns and proportional distributions of study sites and studied tree species across forest biomes (FAO, 2022). Specifically, for counting the frequencies of identified species and genera, species frequency was recorded once per species per study, whereas genus frequency was recorded once per unique species within that genus per study (e.g., *Pinus strobus* and *Pinus resinosa* identified within a single study were counted as two genus-level frequencies). When a single study reported species data from multiple, distinct study sites or regions, these datasets were treated separately for frequency calculations.

In addition, we refined the unit of record from the publication-level to the level of each individual model reporting test performance, hereafter referred to as an *identification task*. This refinement was necessary because a single study often encompasses multiple distinct modeling experiments (e.g., comparisons across model architectures or across different input data types), each

associated with its own training data source, deep learning approach, and evaluation performance. Recording each identification task individually allowed us to systematically quantify the frequency and proportional use of different data sources and modeling frameworks, thereby providing a more precise characterization of the current state of the field. Furthermore, treating each independent identification task as a separate record with its own reported accuracy enabled within-study comparative analyses. Specifically, to quantify the impact of remote sensing data (e.g., data type, data fusion, and temporal resolution) on TSI model performance, we compiled studies that conducted controlled experiments, extracted absolute model performance ($\Delta = Performance_{Proposed} - Performance_{Baseline}$), and calculated the relative differences (Δ_{Rel}) in performance between control groups and baseline models (Eq. 1; Supplementary Table S1 – S4).

$$\Delta_{Rel} = \frac{Performance_{Proposed} - Performance_{Baseline}}{Performance_{Baseline}} \times 100\% \quad \text{(Eq. 1)}$$

where $Proposed$ is the accuracy of the proposed model, $Baseline$ is the accuracy of the baseline model. Impact of hyperspectral, multispectral, and RGB-NIR (red, green, blue, and near-infrared), model performance based on RGB imagery served as the baseline; Impact of data fusion, model performance based on single-imagery data served as the baseline; Impact of multi-temporal data, model performance based on single-temporal data served as the baseline. Model performance (F1-score or Overall Accuracy) was held identical for each paired comparison within a study.

All identification tasks included in the main meta-database were required to satisfy the same five eligibility criteria applied at the study level. For instance, if a study primarily used imagery data but also contained comparative experiments using only LiDAR data, only the imagery-based identification tasks were retained. The resulting database comprises 28 metadata attributes, organized into four key categories (Supplementary Table S5): (1) forest: the location of study sites, biome designation, identified species and genera using scientific binomial names, and the total number of identified classes; (2) data sources: we identified whether the study used single imagery or data fusion, imagery data types (e.g., RGB, multispectral), spatial resolution, data acquisition platforms, and multi-temporal data usage; (3) deep learning models: the computer vision tasks employed (e.g., object detection, instance segmentation) and the specific model framework and model architecture; (4) model performance for each identification, including precision, recall, F1-score, overall accuracy, and Kappa, was recorded. When specific information was not explicitly reported, missing information was denoted as “NA”. Additionally, the complete metadata table also contains shallow machine-learning identification tasks reported as comparators in otherwise eligible studies (Supplementary Table S6, Identification ID beginning with 1060). These records were retained to support the within-study performance comparison between shallow machine learning and deep learning presented in Section 3.3 and Supplementary Table S4. Note that they were analytically separated from the 1034 deep learning-based identification tasks that constitute the main meta-database and were excluded from all other descriptive statistics and meta-analyses.

3. Results and discussion

3.1. Global and taxonomic patterns

TSI research covered all five major forest biomes, but 83% of studies were concentrated in temperate and subtropical regions (Fig. 2a, b). This geographic imbalance contrasts with global tree diversity: Central and South America and South Asia contain nearly 20,000 tree species, compared with fewer than 10,000 in North America, North Asia, and Europe (Cazzolla Gatti et al., 2022). The discrepancy likely reflects differences in species richness (Cazzolla Gatti et al., 2022; FAO and UNEP, 2020), economic relevance (Hajjaji et al., 2022), research investment and capacity (Bartlett et al., 2017; Boshoff et al., 2024), and species identifiability from aerial imagery (Grabska et al., 2020).

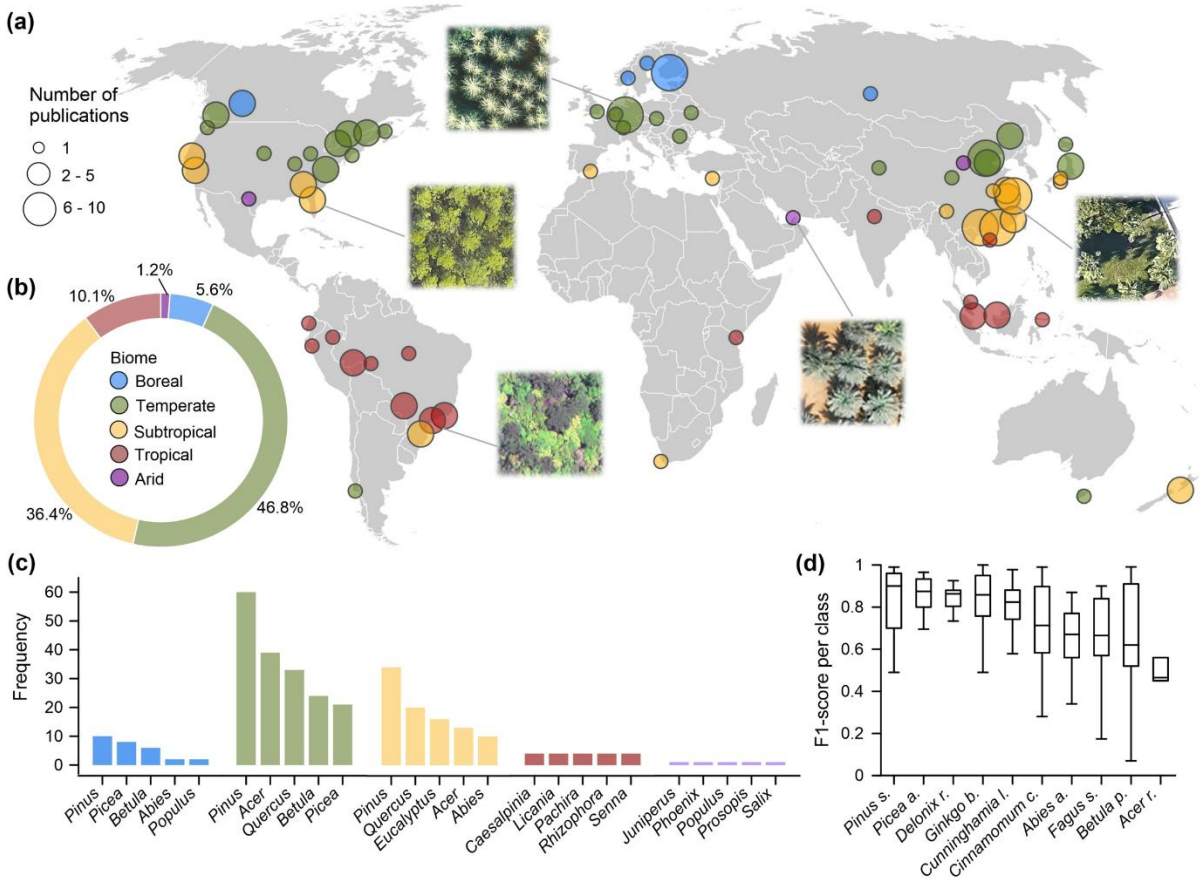


Fig. 2. Global patterns of crown-level tree species identification research. (a) Global map showing the number of publications per site (polar regions omitted), with example aerial images of a temperate conifer forest (Schiefer et al., 2020), a subtropical mixed forest (obtained from Google Maps), a tropical rainforest (La Rosa et al., 2021), an arid palm plantation (Gibril et al., 2021), and a subtropical urban forest (Miao et al., 2024). (b) Proportional distribution of identifications across the five biomes. (c) The five most frequently identified genera in each biome. (d) The 10 most frequently identified species and their per-class F1-scores. Full names of the species (ranked from left to right by median F1-score) are *Pinus sylvestris*, *Picea abies*, *Delonix regia*, *Ginkgo biloba*, *Cunninghamia lanceolata*, *Cinnamomum camphora*, *Abies alba*, *Fagus sylvatica*, *Betula pendula*, and *Acer rubrum.*

The reviewed studies covered 384 species from 213 genera, with strong differences in taxonomic representation among biomes (Fig. 2c; Supplementary Table S7). Only four and eight species were

studied in arid and boreal regions, respectively, compared with 41 in tropical, 181 in temperate, and 199 in subtropical forests. In boreal forests, TSI focused mainly on *Pinus*, *Picea*, and *Betula*; although only eight species were studied, these include many dominant boreal taxa (Pfadenhauer and Klötzli, 2020) that are ecologically important and visually distinctive (Bradshaw and Warkentin, 2015; Shanin et al., 2014).

Tropical TSI was particularly species-selective: 55% of 103 identification tasks targeted one or two species, mainly in plantations or orchards (Supplementary Table S6). These were often economically valuable taxa used for food, medicine, rubber, or oil (Arce et al., 2021; Ferreira et al., 2021; Lee et al., 2024). Urban forests and plantations also provide simpler spatial structures and more accessible reference data, whereas natural rainforests, mountain forests, and mangroves combine complex canopies with difficult field access (Beloiu et al., 2023). Studies identified up to 40 species in temperate urban forests (Aygunes et al., 2021), nine species in tropical urban forests (Martins et al., 2021), and seven fruit tree subspecies in plantations (L. Xu et al., 2024). Thus, tropical TSI still captures only a small fraction of the diversity found in species-rich natural forests.

Within individual datasets, substantial class imbalance occurred: in 27% of reviewed studies, the largest species class contained more than ten times (10:1) as many samples as the smallest (Supplementary Table S6). This partly reflects naturally uneven species abundance (Yuhong Gong et al., 2025; B.G. Weinstein et al., 2023). Among the ten most frequently studied species, *Pinus sylvestris* and *Picea abies* showed among the highest per-class F1-scores, while other high-performing species, including *Delonix regia*, *Ginkgo biloba*, and *Cunninghamia lanceolata*, have distinctive crown characteristics (Fig. 2d; Supplementary Table S8). Reported performance may therefore be biased toward well-represented and visually distinctive species, while performance for rare or visually similar taxa remains less certain.

Addressing the geographic and taxonomic gaps in TSI requires both expanding reference data in underrepresented regions and improving model transferability. Tropical forests of the Global South should be a priority for new species-level reference data and remote sensing studies. In parallel, transfer and incremental learning could enable knowledge from data-rich temperate and subtropical regions to be extended to data-scarce regions (Box 1). The high genus overlap between subtropical and temperate forests enables evaluation of cross-biome transfer (Fig. 2c; Supplementary Table S7). Equitable international collaboration will be essential to strengthen research capacity and scientific participation in currently underrepresented regions (De Lima et al., 2022; Gessler et al., 2024).

3.2. Remote sensing data

3.2.1. Aerial imagery as the baseline

Overall, 83% of identification tasks relied on a single data source, whereas only 17% combined multiple modalities (Fig. 3). Among studies using imagery alone, standard true-color RGB imagery accounted for 62% of all inputs, followed by multispectral (10%), hyperspectral (9%), and RGB-NIR imagery (2%) (Fig. 3a). The predominance of RGB reflects its widespread availability, low acquisition costs, and relatively simple processing workflow. In addition, RGB imagery generally

provides the finest spatial resolution among the reviewed optical data types (Fig. 3b), enabling detailed characterization of crown morphology, texture, and color, which are fundamental cues for species discrimination (Kattenborn et al., 2021; Schiefer et al., 2020). Correspondingly, models trained solely on RGB imagery achieved a mean F1-score of 0.78 across studies, with 59% reporting F1-scores ≥ 0.80 (Supplementary Table S6), demonstrating that RGB imagery alone provides a strong baseline for crown-level tree species identification.

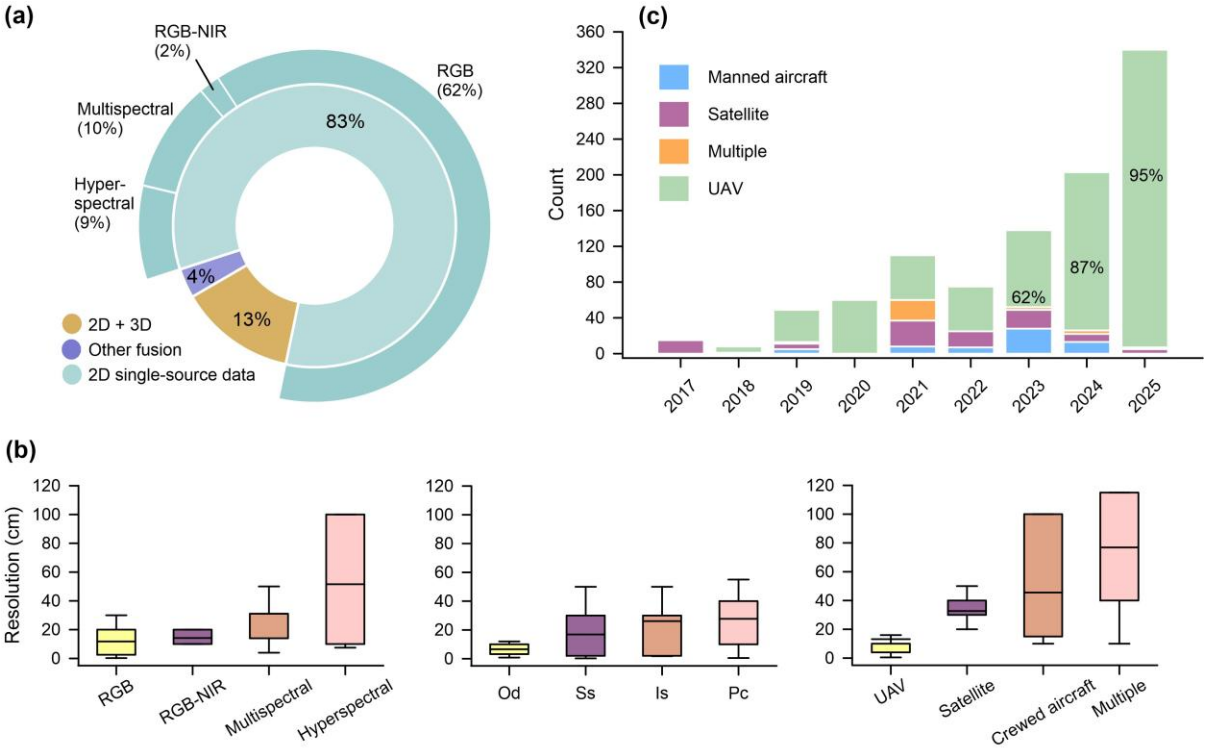


Fig. 3. Usage of remote sensing data in crown-level tree species identification. (a) Proportional distribution of model input data types in reviewed identifications. The inner circle represents the proportions of three broad data types: 2D single data source, data fusion of 2D + 3D, and other fusion. The outer circle further categorizes 2D single data sources into hyperspectral, multispectral, RGB-NIR, and RGB. (b) The average spatial resolutions across remote sensing imagery types, computer vision tasks (Od = object detection, Ss = semantic segmentation, Is = instance segmentation, Pc = patch-wise classification), and data acquisition platforms. (c) Annual trend of usage of each data acquisition platform.

3.2.2. The critical role of spatial resolution and platform

Spatial resolution is a critical determinant in TSI performance, which is one of the prerequisites of precise crown segmentation. 94% of reviewed identification tasks used imagery with a resolution of ≤ 50 cm, and 57% used a resolution of ≤ 10 cm (Supplementary Table S6). The most fine-grained imagery (0.22 cm) was from UAVs (Soltani et al., 2024), whereas the coarsest resolution (up to 200 cm) mostly originated from WorldView satellite imagery (Ferreira et al., 2021; Thapa et al., 2024). Multiple studies reported a degradation in model performance as spatial resolution increased beyond 10 cm (Egli and Höpke, 2020; Lin et al., 2019; Schiefer et al., 2020; Zhong et al., 2024). This decline was more pronounced for broadleaf tree species compared to conifers, suggesting stricter resolution requirements for structurally complex canopies (Schiefer et al., 2020). Crown-level identification requires imagery with spatial resolution finer

than the scale of diagnostic crown features, as it relies on extremely fine-scale structural information such as leaf and branch arrangement, canopy shape, shading, and texture. As spatial resolution coarsens, this fine-grained information is smoothed and aggregated away, thereby weakening the discriminative capacity of computer vision models. This sensitivity appears particularly acute for object detection tasks (Fig. 3b), whose workflow of first localizing a bounding box and then predicting the class highly depends on visually distinct and complete object boundaries (Tong and Wu, 2022). This pattern (Fig. 3b), however, also reflects differences in the data sources preferentially associated with each task type: very-high-resolution imagery tends to be favored for detection tasks (mean resolution = 6 cm), whereas relatively coarser resolution is more commonly adopted as an initial choice for patch-wise classification (mean resolution = 31 cm).

The choice of data acquisition platform in TSI studies also reflects this demand for high spatial resolution. Accordingly, across all reviewed research, UAVs constitute the substantial majority (80% overall, and 95% in 2025) (Fig. 3c), providing an average spatial resolution of 13 cm (Fig. 3b). This trend aligns with broader literature (Pal et al., 2024; Che Zhang et al., 2023), which attributes the appeal of this lightweight, close-range platform to several compelling advantages: capacity to provide high resolution at sub-centimeter level, flexible sensor configurations, and customizable acquisition schedules (Radočaj et al., 2022; H. Yao et al., 2019). Additionally, their relatively low cost and ease of deployment have made them a preferred tool for small-scale, local TSI research (Xuzhan Guo et al., 2021).

Despite the dominance of UAVs, satellite imagery (15% of identifications), primarily from WorldView and Planet (Supplementary Table S6), remains advantageous for regional and global-scale data with high temporal resolution. Meanwhile, several advancements are narrowing the resolution gap between platforms: recent initiatives in low Earth orbit constellations aiming to deliver 10-cm satellite imagery, and the growing use of AI-based enhancement techniques (e.g., super-resolution) to refine existing satellite image resolution (Lepcha et al., 2023). Importantly, high-resolution UAV observations serve as valuable local training data to calibrate and enhance satellite-based large-scale TSI models (Kattenborn et al., 2019), pointing toward an integrated, cross-platform framework as the future of TSI research.

3.2.3. Spectral gains and trade-offs

Moving beyond visible light, 21% of identification tasks investigated additional spectral information, namely RGB-NIR, hyperspectral, or multispectral imagery (Fig. 3a). Across 22 direct comparisons of additional spectral bands with RGB, 82% showed improved performance (mean $\Delta_{Rel} > 0$) (Table 1). Additional spectral information, particularly hyperspectral data, provides biochemical and phenological information related to leaf pigments, greenness, and water content that can aid species discrimination (Féret et al., 2017; Jacquemoud et al., 2009; Lassalle et al., 2023; Z. Yao et al., 2023). The benefit was particularly evident for fine-grained classification: Xu et al. (2024) reported a 9% absolute improvement over RGB for interspecific classification, increasing to 35% at the subspecies level. Additional spectral information may therefore become more valuable when target classes are visually similar in RGB, as in subspecies-level classification.

Spectral gains, however, involve important spatial and methodological trade-offs. Multispectral and hyperspectral sensors are generally more costly and complex to calibrate, and provide coarser spatial resolution than comparable RGB systems (Vu-Duc et al., 2025; Xiong et al., 2025), potentially reducing the crown structure and texture information important for TSI. Additional bands can also limit the direct use of models pretrained on large RGB datasets such as ImageNet (Ahlswede et al., 2023; Ecke et al., 2024). Although manual, PCA-based, and deep learning approaches have been explored for band selection (Miyoshi et al., 2020; Z. Yao et al., 2023), which spectral regions provide meaningful gains for particular species and forest conditions remains unclear.

Table 1. Relative performance differences among remote sensing data configurations. Relative difference analysis for comparing additional spectral bands against RGB imagery, multimodality against 2D single data source, and multi-temporal against single-temporal data. No. = the number of paired comparisons (comparison pairs). Relative and absolute performance differences were calculated using either overall accuracy or F1-score, depending on data availability. For each paired comparison, the same metric was used for both model performances. Relative difference was calculated using Eq. 1 (Section 2.2 of Materials and Methods).

Baseline	Comparison	No.	Relative difference (%)				Absolute difference			
			Min.	Max.	Mean	SD	Min.	Max.	Mean	SD
RGB	Hyperspectral	10	-0.10	328.90	182.80	144.20	0.00	0.62	0.38	0.23
	Multispectral	7	0.41	335.29	49.55	126.01	0.00	0.63	0.10	0.23
	RGB-NIR	5	-1.69	304.81	61.00	136.31	-0.01	0.57	0.11	0.26
2D	2D + 3D	58	-9.02	344.07	12.19	52.01	-0.07	0.33	0.02	0.07
	Other	30	-7.58	36.84	4.62	10.02	-0.05	0.21	0.03	0.06
Single-temporal	Multi-temporal	45	-4.64	60.00	17.31	17.96	-0.04	0.33	0.11	0.10

3.2.4. Integrating multimodal data

Multimodal fusion was used in 17% of TSI tasks, primarily combining imagery with 3D LiDAR data (13%), while 4% fused additional 2D imagery or image-derived metrics (Fig. 3a). Both fusion types improved performance on average relative to single 2D inputs (Table 1). Among 2D combinations, UAV-RGB with satellite multispectral imagery was most common (Aygunes et al., 2021; Xianfei Guo et al., 2022; Y. Sun et al., 2019), combining fine spatial detail with complementary spectral and temporal information. For 3D fusion, CHMs and DSMs were most common (Ecke et al., 2024; Y. Li et al., 2022; Sivanandam and Lucieer, 2022), while some studies incorporated LiDAR-derived intensity, curvature, or leaf area index (Ferreira et al., 2023; Ferreira et al., 2024; Yulin Gong et al., 2024). 3D data used only for crown delineation during pre- or post-processing were not considered data fusion here (Section 3.3).

Although 3D fusion improved performance on average, nearly 40% of the 58 paired comparisons showed no improvement or performance decline (Supplementary Table S2). We considered 3D data as fusion only when used as model input, excluding its use for crown delineation during pre-

or post-processing (Section 3.3). 3D data can complement optical imagery with canopy height and structural information, supporting crown localization in vertically complex forests (Zhong et al., 2024) and separation of canopy from understory vegetation (Imangholiloo et al., 2023). Limited or negative gains may occur when structural information is already represented by optical cues (Nezami et al., 2020; Sothe et al., 2020), species differ little in crown structure (Ferreira et al., 2023; Ferreira et al., 2024), LiDAR point density is insufficient (Nezami et al., 2020), or LiDAR and imagery are misaligned. Thus, the benefit of 3D fusion depends on the complementarity and quality of the added information rather than the addition of 3D data itself.

Depending on the stage of integration, fusion strategies are generally categorized as early fusion (input level), middle fusion (feature level), or late fusion (decision level) (Dollinger et al., 2024; Ghassemian, 2016). In the reviewed TSI studies, however, only early and middle fusion were identified. Early fusion dominated the reviewed tasks (84%) but produced only a 3% mean performance gain, whereas middle fusion accounted for 16% but achieved a substantially larger mean gain of 51% (Supplementary Table S2). Early fusion directly stacks modalities at the input level, making it sensitive to spatial misalignment and differences in resolution (Pohl and Van Genderen, 1998; Z. Wang et al., 2020). In contrast, middle fusion extracts modality-specific features before integration, allowing complementary information to be retained and weighted more effectively. This is particularly relevant when combining structurally different data, such as RGB and CHM, where a shared backbone may underuse weaker but informative height features (Y. Li et al., 2022). These results suggest that future TSI research should focus not only on adding complementary data sources, but on how and where their information is integrated within the model.

In future TSI work, effective data fusion requires careful consideration of four key factors: (1) ensuring the added modality provides genuinely complementary information to avoid unnecessary model complexity; (2) accurate co-registration and harmonization on spatial resolution and timestamp across modalities; (3) designing deep neural network architectures capable of accommodating the distinct characteristics of each modality; and (4) implementing modality- and task-specific preprocessing, including appropriate data augmentation.

3.2.5. The importance of multi-temporal data

Multi-temporal data can capture phenological information, which provides strong cues for distinguishing tree species, yet, only 7% of the identification employed multi-temporal data (Supplementary Table S3, S6). Among these, six publications systematically compared the influence of multi-temporal against single-temporal data on model performance, all of which demonstrated a positive impact (Table 1). This gain may reflect phenological traits, such as color and foliation status of trees, which provide a distinctive spectral signature for species classification (Xianfei Guo et al., 2022; Lei et al., 2022; Veras et al., 2022). Consequently, multi-seasonal data facilitate more accurate species identification. This also highlights that for single-temporal data acquisition, the choice of season is paramount and highly dependent on the target forest ecosystem (Lei et al., 2022; Soltani et al., 2024; Thapa et al., 2024). Therefore, a strategic

selection of the data acquisition season, tailored to the specific phenological characteristics under investigation, is necessary for maximizing TSI accuracy.

3.3. Deep learning approaches for tree species identification

Deep learning is a subfield of machine learning characterized by hierarchical architectures in which successive layers apply linear transformations and non-linear activations to learn increasingly abstract and task-relevant representations from high-dimensional data (LeCun et al., 2015). During iterative supervised training, deep neural networks are optimized end-to-end through the joint use of a loss function, optimizer, progressively refining both feature extraction and output prediction to improve performance (Rumelhart et al., 1986). Before the application of deep learning, crown-level tree species identification relied heavily on expert-defined workflows. Early methods had to enumerate candidate descriptors of crown color, texture, and boundary structure and relate them manually to the spectral properties of remote sensing imagery (Fournier et al., 1995; Gougeon, 1995; Nagendra, 2001). Shallow machine-learning algorithms, particularly random forests (RFs) and support vector machine (SVMs), made classification more accessible and effective, but generally retained separate feature-engineering, feature-selection, and classification stages (Onishi and Ise, 2021; Yan et al., 2021). Producing spatially explicit object-level outputs could additionally require crown delineation before classification or dedicated post-processing after pixel-wise prediction (W. Li et al., 2018; L. Wang et al., 2021). These workflows become more elaborate when multiple data modalities to be harmonized and represented jointly (M. Sun et al., 2025). Deep learning does not eliminate all preprocessing or post-processing, but it allows feature learning and, depending on the computer vision task, localization, segmentation, and classification to be integrated within a more unified trainable framework.

Among the 133 reviewed studies, 28 reported within-study comparisons between deep learning models and shallow machine-learning methods, most commonly RFs and SVMs (Supplementary Table S4). Two of these studies reported cases in which shallow machine learning performed better (Xianfei Guo et al., 2022; C. Hou et al., 2023), whereas the remaining studies reported an overall advantage for deep learning. Across the latter studies, the absolute performance differences ranged from 0.9 to 48.7 percentage points, with a mean difference of 15.1 percentage points (Supplementary Table S4). Studies commonly attributed superior performances to the capacity of deep networks to learn spatial context and hierarchical spectral-spatial representations directly from imagery (Chowdhury et al., 2025). This capacity was particularly beneficial in heterogeneous scenes and where species exhibited similar spectral signatures or subtle visual differences (X. Chen et al., 2025; C. Hou et al., 2023). That said, the overall advantages discussed do not imply that deep learning is universally preferable to shallow machine learning. Deep learning typically requires larger quantities of high-quality annotations (Galdames et al., 2023; Xianfei Guo et al., 2022), greater computational resources and longer training times (Fu et al., 2024; Olariu et al., 2022), and remains less interpretable than many conventional models (Mäyrä et al., 2021; M. Sun et al., 2025). Therefore, the choice between shallow and deep learning should reflect the availability and quality of training data, computational budget, and task complexity. This review does not treat deep learning as a universal replacement for conventional machine learning. Rather, it focuses on deep learning-based computer vision

because these approaches support a broader of spatial prediction tasks, represent a distinct methodological paradigm within machine learning, and constitute one of the most rapidly developing areas of crown-level TSI research.

3.3.1. Computer vision tasks

Depending on the spatial granularity required of the output (i.e., image-patch label, pixel mask, bounding box, or instance-separated mask), computer vision tasks applied to crown-level tree identification can be grouped into four categories: image patch classification, semantic segmentation, object detection, and instance segmentation (Fig. 4a). These four tasks are represented in relatively comparable proportions across the reviewed literature, with patch-wise classification more prevalent, accounting for 41% of all identification tasks (Fig. 4b).

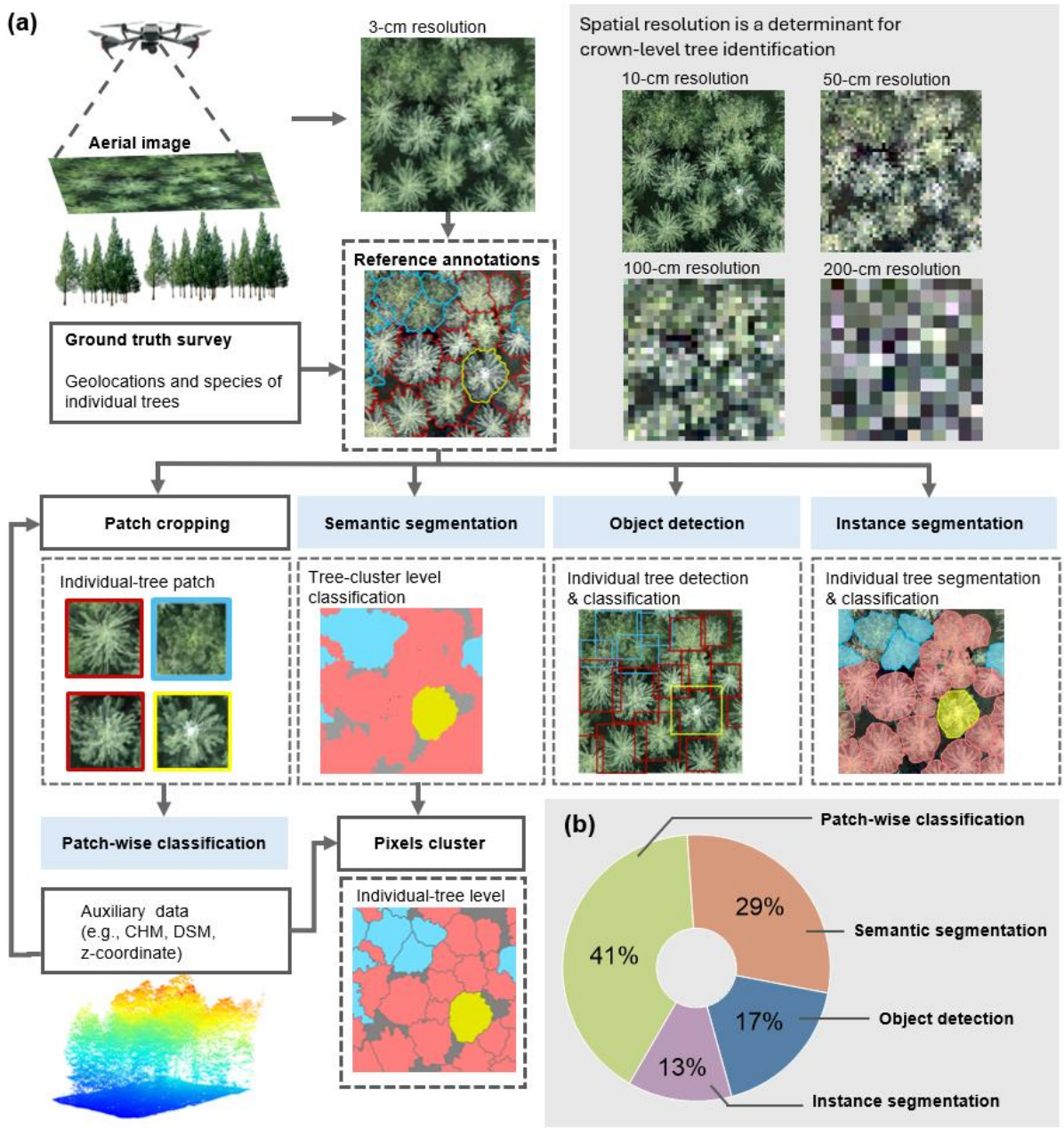


Fig. 4. Computer vision tasks applied to crown-level tree species identification. (a) Workflow of each computer vision task in crown-level tree species identification. Aerial imagery source: TreeAI (Beloiu et al.,

2025). (b) Proportional distributions of computer vision tasks applied in crown-level tree species identification.

Patch-wise classification follows a two-stage workflow: image chips corresponding to individual tree crowns are first cropped during a pre-processing stage (often guided by ancillary geometric references like canopy height models or rule-based segmentation algorithms (Hartling et al., 2019; Nezami et al., 2020)), after which each chip is independently classified (Fig. 4a). This approach remains prevalent due to its intuitive workflow and the flexibility it affords in managing training data. Because the training unit is defined as a one-to-one mapping between an image chip and a class label, this structure enables fine-grained control over sample quality within each class and facilitates the application of targeted training strategies, such as data augmentation and weighted sampling.

At the same time, patch-wise classification simplifies the learning task itself: by cropping each crown into an isolated chip, it substantially reduces, or in some cases entirely removes, interference from background context and inter-crown spatial interactions (Onishi et al., 2022). Because of this task simplicity, the maximum number of classes that a patch-wise classification model in reviewed studies achieved was notably higher than in other computer vision tasks, up to 58 classes (Onishi et al., 2022). Also, because the classification step performs no localization of its own, the resulting model output more directly reflects how differences in the spectral signature within a given crown relate to species-level classification, which is advantageous for quantitative analysis and model interpretability. However, both the inputs and outputs of patch-wise classification are independently labeled image chips lacking spatial continuity with one another. In practical applications, this approach requires that tree crowns in the target area first be accurately delineated. This dependency on site-specific pre-processing and external crown detection algorithms diminishes the overall scalability and automation of the workflow, and the output fundamentally lacks spatial context for mapping large orthomosaics.

Semantic segmentation, as the second most frequently used computer vision task (29%) (Fig. 4b), operates on the principle of classifying every image pixel. Architecturally, semantic segmentation is most commonly implemented via fully convolutional encoder-decoder networks, with the usage of U-Net and DeepLab together accounting for 56% of semantic segmentation studies in this review (Table 2), wherein a downsampling pathway extracts hierarchical spatial features and a corresponding upsampling pathway restores full input resolution, yielding a coherent per-pixel class prediction map end-to-end. Because this formulation assigns class labels independently at the pixel level without incorporating any notion of object instance, adjacent or overlapping crowns of the same species are frequently merged into a single contiguous region, rendering individual crown delineation fundamentally ill-posed in the absence of external instance-separation logic.

Semantic segmentation studies in this review can be grouped into three categories based on their final outputs. First, where distinct gaps exist between tree crowns, as is typical in urban areas, seedling plantations, or arid woodlands, the segmentation output naturally resolves to the individual tree level (Cui et al., 2025; Gibril et al., 2021; X. Liu et al., 2025). Second, many reviewed

studies do not resolve segmentation to individual crowns but instead operate at the level of continuous, mono-species crown clusters. We contend that, aside from applications explicitly requiring accurate crown counts, cluster-level maps delineating precise cluster boundaries are not inherently inferior to maps resolving individual instances; rather, in certain forest settings, this represents a reasonable trade-off among technical difficulty, annotation cost, and practical need (Soltani et al., 2024; L. Wang et al., 2021). For example, in tropical rainforests or densely closed-canopy mountain forests, where even in-situ enumeration of individual stems is hardly feasible, the precise location and spatial extent of a crown cluster already carries meaningful ecological value (X. Chen et al., 2025; Cheng et al., 2024; Chowdhury et al., 2025; X. Wang et al., 2024). Finally, pixel-wise outputs can also serve as the basis for subsequent segmentation or aggregation into individual crowns via object recognition or post-processing methods, such as majority voting, distance mapping, or watershed segmentation, with numerous reviewed studies affirming the effectiveness of this approach (Ferreira et al., 2020; Fu et al., 2024; Martins et al., 2021; Tagle Casapia et al., 2025) (Fig. 4a). This reliance on a separate processing stage, nevertheless, remains a limitation, as it constrains full automation and shifts the burden onto custom pipelines, which directly motivates the development of instance segmentation approaches.

Instance segmentation extends semantic segmentation by introducing object-level identity into the prediction task: rather than assigning each pixel only to a semantic class, the model must additionally determine which individual tree that pixel belongs to. The dominant paradigm in this review is Mask R-CNN and its variants, accounting for 49% of instance segmentation tasks, followed at a considerable distance by Swin Transformer-based frameworks (15%) (Table 2). Mask R-CNN operates as a two-stage, proposal-based framework: a region proposal network first generates candidate bounding boxes likely to contain an object, after which the ROIAlign mechanism extracts fixed-size feature representations for each proposal, and parallel network branches then predict the tree species, refine its bounding box, and generate a pixel-wise binary mask specific to that tree crown (K. He et al., 2017). Because each candidate proposal is processed independently, adjacent or partially overlapping tree crowns, which semantic segmentation would merge into a single contiguous region, can be delineated as distinct, individually bounded objects, directly resolving the instance-ambiguity limitation discussed above.

This capacity to output individually delineated, countable crown masks confers several advantages. First, it enables simultaneous crown counting, localization, and species-level classification in a truly end-to-end manner, closely matching the granularity of field-based tree inventories. Second, because each predicted mask is tied to an explicit object instance, downstream ecological applications and research, such as relating crown area to biomass via allometric equations (Hiernaux et al., 2023), can be performed directly on the output of instance segmentation models, without requiring post-hoc steps. However, these advantages come at a cost. Instance segmentation requires annotating the precise contour of each individual crown as a distinct mask, a labeling effort far greater than that required for patch-level labels (Benenson et al., 2019). This more demanding annotation requirement is compounded by greater architectural complexity, which in turn incurs higher computational cost during both training and inference.

This point is also reflected at the architectural level: whereas patch-wise classification is most commonly implemented using a single, standalone backbone (predominantly ResNet), instance segmentation requires substantially more elaborate, multi-stage architectures like Mask R-CNN and Transformers (Table 2).

Object detection constitutes a relatively distinct computer vision task, whose output is a class-labeled bounding box localizing each object. As such, it can similarly achieve crown-level localization, counting, and classification simultaneously, though without delineating the precise boundary of each crown. In this sense, object detection occupies a middle ground between patch-wise classification and instance segmentation, combining the comparatively low annotation burden and computational cost of the former with much of the streamlined, single-step workflow of the latter (Diez et al., 2021). The practical accessibility of object detection is further reinforced by the availability of numerous open-source, lightweight, and user-friendly frameworks, such as Ultralytics's YOLO, SSD, and FCOS. Particularly, YOLO accounts for 55% of reviewed object detection studies (Table 2), owing to its ease of deployment, intuitive hyperparameter tuning, and demonstrated robustness in forestry scenes.

Table 2. The five most frequently used deep learning frameworks of each computer vision task in the reviewed crown-level tree species identification tasks, with their frequency and percentage.

Computer vision task	Deep learning framework	Frequency	Percentage (%)
Patch-wise classification	ResNet	94	22.43
	Custom CNN	78	18.62
	DenseNet	68	16.23
	3D-CNN	26	6.21
	EfficientNet	24	5.73
	Other	129	31.81
Semantic segmentation	UNet	98	32.56
	DeepLab	71	23.59
	ResNet	25	8.31
	ResUNet	19	6.31
	SegFormer	15	4.98
	Other	73	24.22
Instance segmentation	Mask R-CNN	64	49.23
	Swin Transformer	19	14.62
	YOLO	15	11.54
	Cascade R-CNN	4	3.08
	Custom GNN	4	3.08
	Other	24	18.48
Object detection	YOLO	100	54.64
	Faster R-CNN	29	15.85
	Inception	13	7.1
	RetinaNet	9	4.92
	ResNet	8	4.37
	Other	24	13.15

Object detection in TSI is particularly sensitive to training data quality and crown separation. Accurate classification depends on well-localized bounding boxes, placing high demands on spatial resolution where adjacent crowns overlap (Fig. 3b). Incomplete annotations, such as missing labeled trees in an image chip, further degrade performance because unlabeled trees are implicitly treated as background during training (Adhikari et al., 2021; M. Xu et al., 2019). Finally, rectangular bounding boxes poorly represent irregular or overlapping crowns, introducing pixels from neighboring trees and confounding species classification.

Comparative studies show no consistent superiority of any computer vision task across applications (Korznikov et al., 2023; Chong Zhang et al., 2022). Task selection should instead reflect the required output granularity, target forest, annotation availability, and computational resources (Table 3). Future development should focus on increasing automation and robustness, either by integrating detection or segmentation models such as DeepForest (B.G. Weinstein, Marconi, Aubry-Kientz, et al., 2020), Detectree2 (Ball et al., 2023), DETR (Ambrosio Da Silva et al., 2026), or SAM (Que et al., 2026) into classification workflows or by developing object detection and instance segmentation approaches or embedding mechanisms that remain reliable under limited and imperfect training data.

Table 3. Summary of different computer vision approaches in reviewed studies.

Approach	Advantages	Limitations
Patch-wise classification	● High flexibility in combining segmentation and classification methods. ● High flexibility in training and testing data division. Incomplete and missing ground truth labeled objects can be easily removed. ● Requires simpler models.	● Creating patches of individual crowns is inefficient. ● Details are limited to patch-level, cannot resolve individual pixels or instances. ● Relies heavily on external CHMs/DSMs for pre-segmentation.
Semantic segmentation	● Efficient at the tree-cluster level, providing precise tree-cluster extents and locations. ● Produces coherent classification maps on large image tiles. ● Requires simpler models.	● Requires post-processing for individual crown delineation.
Object detection	● Simultaneous crown localization, quantification, and classification. ● Good and cost-effective performance in simple forests. ● Requires less annotation effort than masks.	● Sensitive to high-quality annotations. ● Limited precision in crown boundaries. ● Less effective in dense or heterogeneous forests.
Instance segmentation	● Simultaneous crown localization, delineation, quantification, and classification.	● Annotation-intensive. ● Higher computational demand.

	● Good performance in dense and complex forests. ● Strong transferability potential.

CHM = canopy height model; DSM = digital surface model.

3.3.2. Convolutional, attention-based, and transformer architectures

CNNs are among the most representative model families within deep learning (LeCun et al., 2015), it also remains dominant across crown-level TSI, accounting for 77% of identification tasks, while a further 15% use CNN backbones with attention mechanisms (Fig. 5; Supplementary Table S6). Attention modules such as Squeeze-and-Excitation (Z. He and He, 2021), the Convolutional Block Attention Module (Ma et al., 2024), and task-specific variants (Cai et al., 2025; B.G. Weinstein et al., 2023) help emphasize informative spatial or spectral features while suppressing background information. Their use is particularly common in object detection and instance segmentation, often through adapted DeepLab or YOLO frameworks (B. Hou et al., 2025; Z. Sun et al., 2025; Q. Wang et al., 2025).

Beyond the dominant CNN-based architectures, Transformer-based models are emerging across TSI tasks (Fig. 5). Representative frameworks include Swin Transformer, Vision Transformer, and SegFormer (Huang et al., 2023; Liang et al., 2025). Unlike CNNs, which primarily build context through local convolutions, Transformers use self-attention to capture relationships across larger image regions (Dosovitskiy et al., 2020; Vaswani et al., 2017). Recent studies increasingly combine model families rather than relying on single architectures. Ensemble (Briechle et al., 2021), hierarchical (Lei et al., 2022; S. Liu et al., 2026), and hybrid CNN-Transformer frameworks seek to combine local feature extraction with broader contextual representation. Examples include CNN-Transformer encoder-decoder architectures (X. Zhang et al., 2025), YOLO coupled with Segment Anything for crown localization and mask refinement (Que et al., 2026), and Mamba-based models designed to capture long-range dependencies at lower computational cost (X. Zhang et al., 2025). Overall, these developments indicate increasing architectural diversification in TSI, with growing use of modular backbones, attention blocks, decoders, prompting mechanisms, and task-specific heads, although evidence for consistent performance gains remains limited.

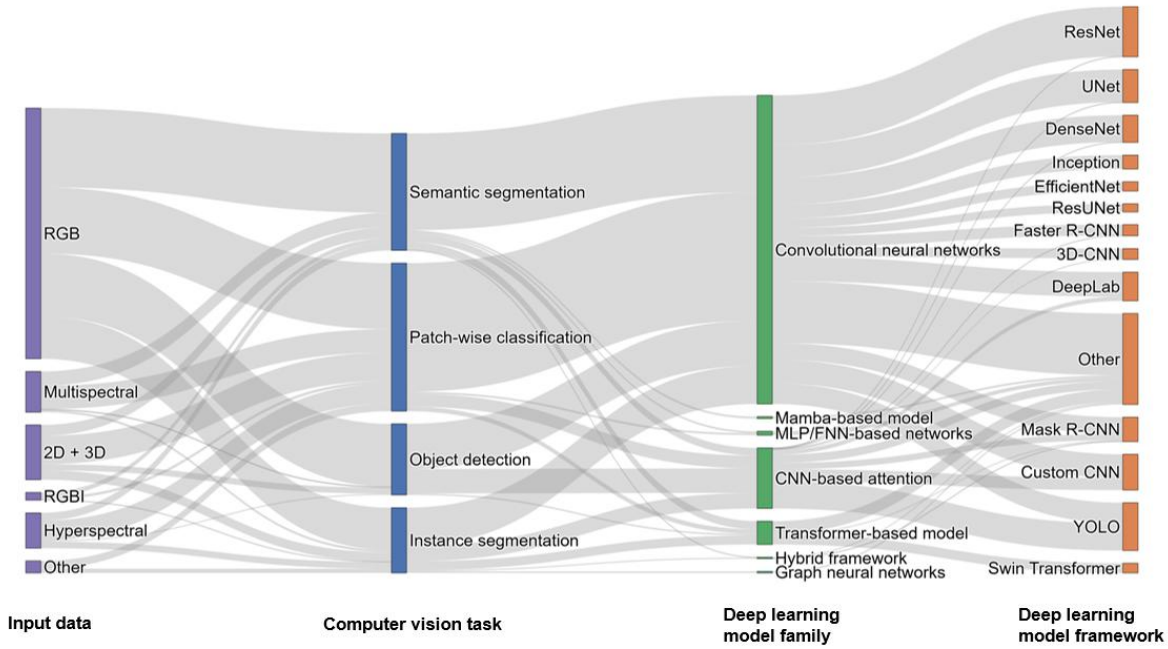


Fig. 5. Sankey diagram showing the proportional distribution and associations among input data types, computer vision tasks, deep learning model families, and model frameworks used in the reviewed tree species identification studies.

3.4. Challenges and perspectives

Deep learning has substantially advanced crown-level tree species identification, but the task remains challenging because species identity must be inferred from highly variable and spatially complex visual observations. Even within a single species, individual crowns can differ markedly in color, texture, shape, size, phenological condition, and boundary appearance. Trees also frequently occur in dense, overlapping canopies, where crown boundaries are ambiguous and neighboring species contribute mixed spectral and textural information. These properties distinguish crown-level TSI from many conventional computer vision applications involving more regular object geometries or more clearly separated classes. They also compound the general limitations of deep learning, including dependence on extensive and representative annotations, sensitivity to class imbalance and domain shift, and limited transferability across forests, seasons, sensors, and geographic regions. The following sections examine the data and model limitations that most strongly constrain accurate, robust, and transferable crown-level TSI and discuss the methodological directions that may help address them.

3.4.1. Addressing data limitations

Training-data limitations occur at both species and geographic levels: 27% of studies had >10:1 class imbalance, while 83% were concentrated in temperate and subtropical forests. The robustness of deep learning models is fundamentally contingent on the volume and quality of training data. Data quality, in this context, encompasses not only fidelity but, for classification-related deep learning tasks specifically, also the balance of sample sizes across classes and the richness of intra-class representation (Buda et al., 2018; Mellor et al., 2015). Yet in forestry applications, acquiring large volumes of high-quality data is often costly and logistically

challenging (Fassnacht et al., 2024), owing to variable forest accessibility, naturally imbalanced species distributions, and disparities in the labor and funding available for data collection (Bartlett et al., 2017; Boshoff et al., 2024; Yuhong Gong et al., 2025). As noted in Section 3.1, this gives rise to imbalance at two levels within the TSI domain: a. within-dataset imbalance in sample sizes across species, and b. imbalance in the availability of datasets across different geographic regions. The former constrains model performance and stability, while the latter impedes the progression of TSI research from local case studies toward large-scale, global applications.

Addressing these data availability and imbalance challenges requires open data sharing and standardized, domain-specific databases (Lines et al., 2022). Researchers should deposit datasets on open platforms such as Hugging Face and Zenodo to build community-wide resources; existing TSI databases are summarized in Table 4. Equally important is standardizing annotation and quality control, as inconsistent labels can compromise the completeness, consistency, and taxonomic balance of training data. Key issues include: (1) inconsistent taxonomic systems and class lists (GBIF Secretariat, 2023); (2) inconsistent naming conventions (e.g., *Picea abies* versus *Picea abies* L.); (3) mixed or overlapping taxonomic levels (e.g., *Picea* spp. and *Picea abies*); (4) missing hierarchical class structures (tree > conifer > *Picea* > *Picea abies*); and (5) variable crown-delineation quality, particularly from manual image interpretation (Allen et al., 2025). Incomplete annotation presents an additional problem: unlabeled trees are treated as background, potentially degrading detection and segmentation models. Future TSI databases should therefore combine open data sharing with standardized taxonomy, annotation, and quality-control protocols.

Beyond improving data availability and standardization, deep learning strategies can mitigate remaining data scarcity and imbalance. Data-centric and active learning can improve training data by refining low-quality samples and prioritizing the most informative samples for annotation (Desai and Ghose, 2022; W. Zhang et al., 2024). Models can also be made more tolerant to incomplete or imbalanced labels through pseudo-labeling (B. Hou et al., 2025; Miao et al., 2024), soft sampling, ignore masking (Wu et al., 2018), and adapted attention mechanisms and loss functions (Johnson and Khoshgoftaar, 2019; Simmler et al., 2021; H. Zhang et al., 2020). Emerging multimodal approaches offer another direction by combining forestry-specific knowledge, such as crown morphology and environmental context, with remote sensing imagery through image-text embeddings. Generative models could further augment scarce classes through synthetic crown imagery and annotations (Yun et al., 2026).

To realize the full potential of deep learning on a global scale, the field must prioritize the creation of shared, heterogeneous datasets through community-wide collaboration. Integrating diverse research groups via data hosting platforms and large-scale projects is the only viable path to generate benchmarks that are truly representative of the world's biomes. Such initiatives serve a dual purpose: curating the vast training data necessary for high-performance models while simultaneously establishing best practices for data quality and standardization. This approach has already proven transformative in related domains, exemplified by the 20forK LiDAR dataset (Puliti et al., 2025) and the 3Dtrees.earth (Kilian et al., 2026), which addresses tree species classification with LiDAR data. Examples on the image domain are the global deadtrees.earth initiative (Mosig

et al., 2026), which focuses on tree vitality mapping with drones and satellites, or TreeAI, which crowd-sources image data with tree species annotations (Beloiu et al., 2025). Embracing such collaborative paradigms is essential for bridging the generalization gap in crown-level species identification.

Table 4. Open-access reference datasets for crown-level tree species identification.

No.	Data	Description
1.	NEON Tree Species Predictions (B. Weinstein et al., 2020)	Species predictions at the individual tree level for 100 million trees in the National Ecological Observatory Network, the United States.
2.	Tree detection in UAV LiDAR and RGB image data (Dubrovin et al., 2024)	The dataset contains 3,600 trees from seven species across 10 ground plots in Perm Krai, Russia, accompanied by a LiDAR point cloud and an RGB orthophoto.
3.	Quebec Trees Dataset (Cloutier et al., 2023)	The dataset comprises over 22,000 trees from 20 species and RGB imagery in Quebec, Canada.
4.	TreeAI Global Initiative (Beloiu et al., 2025)	The dataset provides over 100,000 tree annotations across 70 species in COCO format and RGB imagery from diverse locations worldwide.

3.4.2. Model generalization, robustness, and transferability

Generalization, robustness, and transferability describe related but distinct performance dimensions in deep learning for TSI (see Box 1). Current TSI models often generalize well (within their training domain) but show limited robustness and very low transferability across sites, particularly due to domain shift (Kattenborn et al., 2022). Improving transferability is therefore central to addressing geographic and ecological data gaps, allowing knowledge from data-rich regions to support TSI in data-scarce regions without developing independent models for every site. Cross-site performance depends on factors including sensor characteristics, taxonomic overlap, phenology, and forest structural complexity. Transfer learning and domain adaptation can facilitate adaptation to new environments (Chadwick et al., 2024; B.G. Weinstein, Marconi, Bohlman, et al., 2020), while self-supervised pretraining can reduce dependence on labeled data. Continual and incremental learning can further incorporate new species and biomes without retraining from scratch (Van De Ven et al., 2022). Together, these approaches provide a pathway toward universal TSI models capable of operating across species, forests, sensors, and regions.

Box 1 - Key performance concepts in deep learning

Generalization: DL model's ability to perform well on unseen data drawn from the *same* distribution as the training set, such as new crowns of the *same species* within the same forest type (Chiyuan Zhang et al., 2016).

Robustness: The stability of a DL model's performance under perturbations, including changes in illumination, season, view angle, or sensor noise, which are common in aerial imagery and can significantly distort spectral and textural cues (Mei et al., 2024).

Transferability: A model's ability to maintain performance when applied to different forests, biomes, or sensor conditions, where species composition, canopy structure, and imaging geometry may differ substantially from the training data. Transferability does not mean that a model trained on a given species (e.g., spruce) can recognize new species elsewhere. Rather, a transferable model can (i) continue to recognize the same species in new environments, and (ii) reuse its learned visual representations, such as texture, shape, or canopy-structure cues, to be efficiently adapted to different species through fine-tuning, domain adaptation, or continual learning, which all require additional data from the target environment (labeled data for new species in fine-tuning and continual learning, and labeled or unlabeled target-domain data for domain adaptation). Because these situations involve large domain gaps, transferability represents the most challenging performance dimension (Parisi et al., 2019; Tuia et al., 2025).

Domain shift: The mismatch between the statistical properties of training data and those encountered during deployment, often caused by differences in forest structure, species composition, acquisition geometry, seasonality, or sensor characteristics. Domain shift affects all three performance dimensions: it has minimal impact on generalization, moderate impact on robustness, and is the primary cause of poor transferability.

Transfer learning: A method that reuses visual features learned by a pre-trained model to improve performance on a new task or in a new environment, reducing the need for extensive additional training data. Transfer learning is used mainly to improve transferability by counteracting domain shift and can also enhance robustness by promoting more domain-invariant feature learning (Pan and Yang, 2010; Parisi et al., 2019).

3.4.3. Standardizing reporting metrics

Reporting of model performance was highly inconsistent across reviewed TSI studies: F1-score and overall accuracy were the most frequently reported metrics, yet each appeared in fewer than 60% of identification tasks (Supplementary Table S6). This limits direct comparison and benchmarking across studies. Essential dataset information should also be consistently reported, including binomial species names, spectral bands, and spatial resolution.

We therefore recommend a common set of task-specific metrics (Table 5). Precision, recall, and F1-score should provide the baseline across tasks, complemented by mean Average Precision (mAP) at a specified Intersection-over-Union (IoU) threshold for object detection and IoU for semantic and instance segmentation. Macro- and weighted-average metrics should be accompanied by per-class results, particularly for imbalanced datasets. Importantly, these metrics are only comparable when evaluated on independent data that minimize spatial and temporal autocorrelation (Kattenborn et al., 2022; Ploton et al., 2020). Spatial block cross-validation or

comparable approaches should therefore be used to ensure robust evaluation (Ploton et al., 2020; Roberts et al., 2017).

Table 5. Summary of evaluation metrics with respective equations and descriptions.

Evaluation metrics	Equation	Description
Precision	$\frac{TP}{TP+FP}$	The proportion of model-predicted objects that are correct.
Recall	$\frac{TP}{TP+FN}$	The proportion of true objects that are correctly detected by models.
F1-score	$2\times\frac{Precision\times Recall}{Precision+Recall}$	The harmonic mean of Precision and Recall.
IoU	$\frac{Area\ of\ Overlap}{Area\ of\ Union}$	The ratio between the intersecting area and the total combined area of the predicted bounding box (or mask) and the ground truth box (or mask).
AP	$\int_0^1 p(r)dr$	Average precision equals the area under the Precision-Recall curve for each class.
mAP	$\frac{1}{N}\sum_{i=1}^{n} x_{ii}$	Unweighted average AP across all classes.
Overall accuracy	$\frac{1}{N}\sum_{i=1}^{n} AP_i$	The ratio of all correctly classified objects to the total number of true objects across all classes

Note that TP represents the true positive, FP represents the false positive, FN represents the false negative, $p(r)$ represents the maximum precision at a given recall level, n is the number of classes, x_{ii} is the number of correct predictions in class i.

3.4.4. Advances in high spatial and temporal resolution data

The growing availability of open, high-resolution aerial and LiDAR data is rapidly expanding the possibilities for crown-level species identification. Several European countries now provide nationwide or regional very high-resolution aerial imagery (5–25 cm), including Switzerland, Austria, Germany, the Netherlands, Denmark, Poland, Spain, parts of the Nordic countries, and France (Bd Ortho; Klimadatastyrelsen; *Swissimage*), which additionally operate airborne LiDAR programs. Globally, the United Nations Strategic Plan for Forests and the EU Forest Strategy for 2030 highlight the need for harmonized, high-resolution forest monitoring systems to support biodiversity and climate objectives (European commission, 2026). Further, incorporating non-orthorectified, multi-view imagery, combining high-nadir with low-oblique views, has been shown to preserve vertical structure and bark characteristics that improve taxonomic classification (Miao et al., 2024; Russell et al., 2024; Sobhana et al., 2025). Likewise, high-volume leaf- and branch-level texture data from citizen-science photographs can enhance model performance when tested on aerial imagery (Soltani et al., 2022; Soltani et al., 2024).

Achieving global-scale, high-resolution imagery for TSI depends on narrowing the resolution gap between satellite and UAV data. Super-resolution has recently garnered significant attention and offers a promising path forward (Huang et al., 2023; P. Wang et al., 2022). High-ratio super-resolution upscaling still carries uncertainty, and current studies capable of refining sub-meter imagery to the 10 cm resolution required for TSI remain scarce (Huang et al., 2023; Mao et al., 2025). Looking ahead, increasing sub-meter resolution satellite imagery, combined with advances

in super-resolution that can bridge both spatial resolution and coverage gaps, holds the potential to produce continental- or global-scale very-high-resolution imagery. Importantly, such developments would not only improve spatial detail but also enable the integration of multispectral and multitemporal satellite information with UAV data, which would benefit large-scale and real-time TSI research.

3.4.5. Foundation models and interpretability

Foundation models are rapidly emerging as a potential solution for overcoming key challenges in TSI, such as ground truth data scarcity, imbalance, and poor model generalization. While foundation models like CLIP, DINO, and SAM dominate broad computer vision, the remote sensing field has developed specific counterparts, including RemoteCLIP, SpectralEarth, Prithvi-EO, and AlphaEarth (Braham et al., 2025; Brown et al., 2025; F. Liu et al., 2024; Szwarcman et al., 2026). These efforts aggregate a massive collection of Earth observation data and spectral information. For TSI, there are currently two main pathways for applying foundation models: (1) fine-tuning general object detection foundation models using TSI-specific data (Lu et al., 2023; J. Zhang et al., 2025); given the persistent scarcity and imbalance of annotated crown-level datasets, parameter-efficient fine-tuning strategies (e.g., LoRA (Hu et al., 2021), adapter-based tuning (R. He et al., 2021)) are particularly well-suited to this pathway, as they adapt large pretrained backbones to species-specific tasks while mitigating overfitting risk; and (2) combining segmentation-focused foundation models, such as SAM's promotable segmentation capability for crown delineation, with dedicated downstream classification models, thereby allocating specialized, powerful models to their respective tasks (Olsson, 2024; Que et al., 2026).

Vision-language foundation models offer an additional opportunity for rare or previously unseen species, as textual species descriptions could support zero- or few-shot identification. More broadly, self-supervised, contrastive, and zero-shot learning could help address data scarcity and long-tailed species distributions (M. Chen et al., 2025; Yuhong Gong et al., 2025) and can offer abundant inspiration for the future workflow design and training strategies for TSI models (Hauser et al., 2025; Muhtar et al., 2023). Their suitability for crown-level TSI nevertheless remains uncertain, because most remote sensing foundation models are pretrained on coarse- to moderate-resolution imagery and may not capture the fine crown texture and spectral differences required for species discrimination (Bountos et al., 2025; Endres et al., 2026). Developing models and pretraining strategies better suited to crown-level information therefore remains an important research direction.

Explainable AI and Causal AI can address the 'black-box' nature of deep learning in forestry remote sensing (Costanza et al., 2025; W. Zhang et al., 2024). Explainable AI uses feature importance, attribution maps, and attention visualization to identify which spectral or structural features drive predictions and whether they align with ecological understanding (Hassija et al., 2024). This can help identify failure modes, redundant inputs, and opportunities to improve data acquisition and model training. Causal AI addresses a complementary problem: models may learn site- or sensor-specific correlations rather than ecologically meaningful signals, potentially contributing to domain shift and poor cross-site transferability. Causal discovery and

counterfactual reasoning could help distinguish ecological drivers from acquisition-related confounding. Together, Explainable and Causal AI could move TSI beyond prediction toward more ecologically informed and transferable models (Tuia et al., 2025).

4. Conclusion

This review synthesized 133 studies (2017–2025) and 1,034 crown-level tree species identification tasks, providing the first quantitative synthesis of how forest, remote sensing, and deep learning factors jointly shape tree species identification performance. The next frontier for TSI is not incremental improvement of site-specific accuracy, but the development of transferable models that can identify tree species across forests, sensors, and regions. Progress toward universal models would allow knowledge acquired from existing datasets to be retained and extended to new species and environments rather than rebuilding models for each site.

Developing transferable TSI models requires advances in data, remote sensing, and learning strategies. Three priorities emerge: (1) globally representative, standardized, and openly shared reference data that expand taxonomic and ecological coverage; (2) learning strategies capable of adapting to new species and scarce, imbalanced, and long-tailed data; and (3) rigorous evaluation of generalization, robustness, and particularly cross-site transferability. Cost-effective and widely available RGB imagery provides a practical basis for large-scale mapping, while fusion with complementary spectral, temporal, and structural information can improve species discrimination, particularly in complex forests. Together, representative data, multimodal information, adaptive learning, and cross-site evaluation provide a pathway toward increasingly transferable TSI models.

Scalable and transferable tree species identification would provide a new species-level information layer for ecological research, forest monitoring, and management. Individual-tree species information could strengthen forest inventories, biodiversity assessment, species-specific biomass and carbon estimation, and monitoring of responses to drought, pests, disease, and other disturbances. At broader scales, consistent species information could support forest and biodiversity monitoring and reporting under global and regional frameworks, including the UN Strategic Plan for Forests and the EU Forest Strategy for 2030. The long-term impact of TSI therefore extends beyond identifying individual trees: it lies in connecting Earth observation with species-level ecological information from local to global scales.

5. Data availability

The database, including the full list of publications and all extracted data used in the meta-analysis, is provided in the Supplementary Information.

6. References

Adhikari, B., Peltomäki, J., Germi, S.B., Rahtu, E., Huttunen, H., 2021. Effect of label noise on robustness of deep neural network object detectors. In: Habli, I., Sujan, M., Gerasimou, S., Schoitsch, E., Bitsch, F. (Eds), Computer safety, reliability, and security. SAFECOMP 2021 workshops, Springer International Publishing, Cham, pp. 239–250.

Ahlswede, S., Schulz, C., Gava, C., Helber, P., Bischke, B., Förster, M., Arias, F., Hees, J., Demir, B., Kleinschmit, B., 2023. *TreeSatAI Benchmark Archive*: a multi-sensor, multi-label dataset for tree species classification in remote sensing. Earth System Science Data 15 (2), 681–695.

Allen, M.J., Owen, H.J.F., Grieve, S.W.D., Lines, E.R., 2025. Manual labelling artificially inflates deep learning-based segmentation performance on RGB images of closed canopy: validation using TLS. arXiv:2503.14273.

Ambrosio Da Silva, I., Barbalho, S.C.M., Bergamini, L.L., Takahashi, F.S.C., Borges, D.L., 2026. Identification of buriti (mauritia flexuosa) and palmito juçara (euterpe edulis) species using RT-DETR through high-resolution images captured by UAV. In: Castrillón-Santana, M., Travieso-González, C.M., Deniz Suarez, O., Freire-Obregón, D., Hernández-Sosa, D., Lorenzo-Navarro, J., Santana, O.J. (Eds), Computer analysis of images and patterns, Springer Nature Switzerland, Cham, pp. 305–315.

Arce, L.S.D., Osco, L.P., Arruda, M.D.S.D., Furuya, D.E.G., Ramos, A.P.M., Aoki, C., Pott, A., Fatholahi, S., Li, J., Araújo, F.F.D., Gonçalves, W.N., Marcato Junior, J., 2021. Mauritia flexuosa palm trees airborne mapping with deep convolutional neural network. Scientific Reports 11 (1), 19619.

Aygunes, B., Cinbis, R.G., Aksoy, S., 2021. Weakly supervised instance attention for multisource fine-grained object recognition with an application to tree species classification. ISPRS Journal of Photogrammetry and Remote Sensing 176, 262–274.

Ball, J.G.C., Hickman, S.H.M., Jackson, T.D., Koay, X.J., Hirst, J., Jay, W., Archer, M., Aubry-Kientz, M., Vincent, G., Coomes, D.A., 2023. Accurate delineation of individual tree crowns in tropical forests from aerial RGB imagery using mask R-CNN. Remote Sensing in Ecology and Conservation 9 (5), 641–655.

Barbier, S., Gosselin, F., Balandier, P., 2008. Influence of tree species on understory vegetation diversity and mechanisms involved—a critical review for temperate and boreal forests. Forest Ecology and Management 254 (1), 1–15.

Bartlett, A.G., Kanowski, P.J., Van Kerkhoff, L., Byron, R.N., 2017. Identifying factors that influence the success of forestry research projects implemented in developing countries: case study results from Vietnam. Forestry: an International Journal of Forest Research 90 (3), 413–425.

Bd Ortho, L'image géographique du territoire national, la france vue du ciel, https://geoservices.ign.fr/bdortho. (Accessed 11 December, 2025).

Beloiu, M., Heinzmann, L., Rehush, N., Gessler, A., Griess, V.C., 2023. Individual tree-crown detection and species identification in heterogeneous forests using aerial RGB imagery and deep learning. Remote Sensing 15 (5), 1463.

Beloiu, M., Xia, Z., Gessler, A., Kattenborn, T., Mosig, C., Puliti, S., Waser, L., Rehush, N., Cheng, Y., Xinliang, L., Griess, V.C., Mokroš, M., 2025. TreeAI global initiative - advancing tree species identification from aerial images with deep learning. Zenodo. https://doi.org/10.5281/zenodo.14888706.

Benenson, R., Popov, S., Ferrari, V., 2019. Large-scale interactive object segmentation with human annotators. 2019 IEEE/CVF Conference on Computer Vision and Pattern Recognition (CVPR), IEEE, Long Beach, CA, USA, June, pp. 11692–11701.

Blaschke, T., Hay, G.J., Kelly, M., Lang, S., Hofmann, P., Addink, E., Queiroz Feitosa, R., Van Der Meer, F., Van Der Werff, H., Van Coillie, F., Tiede, D., 2014. Geographic object-based image analysis – towards a new paradigm. ISPRS Journal of Photogrammetry and Remote Sensing 87, 180–191.

Boshoff, N., Ngwenya, S., Koch, S., Dudek, J., Strelnyk, O., Costas, R., Uisso, A.J., 2024. Geographical inequalities in global forest science: a bibliometric perspective. Forest Policy and Economics 165, 103250.

Bountos, N.I., Ouaknine, A., Papoutsis, I., Rolnick, D., 2025. FoMo: multi-modal, multi-scale and multi-task remote sensing foundation models for forest monitoring. Proceedings of the AAAI Conference on Artificial Intelligence 39 (27), 27858–27868.

Bradshaw, C.J.A., Warkentin, I.G., 2015. Global estimates of boreal forest carbon stocks and flux. Global and Planetary Change 128, 24–30.

Braham, N.A.A., Albrecht, C.M., Mairal, J., Chanussot, J., Wang, Y., Zhu, X.X., 2025. SpectralEarth: training hyperspectral foundation models at scale. IEEE Journal of Selected Topics in Applied Earth Observations and Remote Sensing 18, 16780–16797.

Brandt, M., Chave, J., Li, S., Fensholt, R., Ciais, P., Wigneron, J.-P., Gieseke, F., Saatchi, S., Tucker, C.J., Igel, C., 2024. High-resolution sensors and deep learning models for tree resource monitoring. Nature Reviews Electrical Engineering 2 (1), 13–26.

Briechle, S., Krzystek, P., Vosselman, G., 2021. Silvi-net – a dual-CNN approach for combined classification of tree species and standing dead trees from remote sensing data. International Journal of Applied Earth Observation and Geoinformation 98, 102292.

Brown, C.F., Kazmierski, M.R., Pasquarella, V.J., Rucklidge, W.J., Samsikova, M., Zhang, C., Shelhamer, E., Lahera, E., Wiles, O., Ilyushchenko, S., Gorelick, N., Zhang, L.L., Alj, S., Schechter, E., Askay, S., Guinan, O., Moore, R., Boukouvalas, A., Kohli, P., 2025. AlphaEarth foundations: an embedding field model for accurate and efficient global mapping from sparse label data. arXiv:2507.22291.

Buda, M., Maki, A., Mazurowski, M.A., 2018. A systematic study of the class imbalance problem in convolutional neural networks. Neural Networks 106, 249–259.

Cai, Y., Gao, L., Jia, C., Liu, X., Wang, G., Tian, Y., 2025. Coniferous tree species classification based on DMCA-unet network model with UAV multispectral imagery. Trees, Forests and People 22, 101026.

Cazzolla Gatti, R., Reich, P.B., Gamarra, J.G.P., Crowther, T., Hui, C., Morera, A., Bastin, J.-F., Miguel, S. de-, Nabuurs, G.-J., Svenning, J.-C., Serra-Diaz, J.M., Merow, C., Enquist, B., Kamenetsky, M., Lee, J., Zhu, J., Fang, J., Jacobs, D.F., Pijanowski, B., Banerjee, A., Giaquinto, R.A., Alberti, G., Almeyda Zambrano, A.M., Alvarez-Davila, E., Araujo-Murakami, A., Avitabile, V., Aymard, G.A., Balazy, R., Baraloto, C., Barroso, J.G., Bastian, M.L., Birnbaum, P., Bitariho, R., Bogaert, J., Bongers, F., Bouriaud, O., Brancalion, P.H.S., Brearley, F.Q., Broadbent, E.N., Bussotti, F., Castro Da Silva, W., César, R.G., Češljar, G., Chama Moscoso, V., Chen, H.Y.H., Cienciala, E., Clark, C.J., Coomes, D.A., Dayanandan, S., Decuyper, M., Dee, L.E., Del Aguila Pasquel, J., Derroire, G., Djuikouo, M.N.K., Van Do, T., Dolezal, J., Đorđević, I.Đ., Engel, J., Fayle, T.M., Feldpausch, T.R., Fridman, J.K., Harris, D.J., Hemp, A., Hengeveld, G., Herault, B., Herold, M., Ibanez, T., Jagodzinski, A.M., Jaroszewicz, B., Jeffery, K.J., Johannsen, V.K., Jucker, T., Kangur, A., Karminov, V.N., Kartawinata, K., Kennard, D.K., Kepfer-Rojas, S., Keppel, G., Khan, M.L., Khare, P.K., Kileen, T.J., Kim, H.S., Korjus, H., Kumar,

A., Kumar, A., Laarmann, D., Labrière, N., Lang, M., Lewis, S.L., Lukina, N., Maitner, B.S., Malhi, Y., Marshall, A.R., Martynenko, O.V., Monteagudo Mendoza, A.L., Ontikov, P.V., Ortiz-Malavasi, E., Pallqui Camacho, N.C., Paquette, A., Park, M., et al., 2022. The number of tree species on Earth. Proceedings of the National Academy of Sciences 119 (6), e2115329119.

Chadwick, A.J., Coops, N.C., Bater, C.W., Martens, L.A., White, B., 2024. Transferability of a mask R–CNN model for the delineation and classification of two species of regenerating tree crowns to untrained sites. Science of Remote Sensing 9, 100109.

Chen, M., Russell, D., Pallavoor, A., Young, D., Wu, J., 2025. Zero-shot tree detection and segmentation from aerial forest imagery. arXiv:2506.03114.

Chen, X., Zhang, X., Zhuang, C., Dai, X., Kong, L., Xie, Z., Hu, X., 2025. An approach for detecting mangrove areas and mapping species using multispectral drone imagery and deep learning. Sensors 25 (8), 2540.

Cheng, Y., Oehmcke, S., Brandt, M., Rosenthal, L., Das, A., Vrieling, A., Saatchi, S., Wagner, F., Mugabowindekwe, M., Verbruggen, W., Beier, C., Horion, S., 2024. Scattered tree death contributes to substantial forest loss in california. Nature Communications 15 (1), 641–653.

Chowdhury, A.I., Heinaro, E., Tanhuanpää, T., Rahman, A.U., Junttila, S., 2025. Mapping large european aspens (populus tremula L.) using national aerial imagery and a U-net convolutional neural network. Remote Sensing Applications: Society and Environment 40, 101755.

Christin, S., Hervet, É., Lecomte, N., 2019. Applications for deep learning in ecology. Methods in Ecology and Evolution 10 (10), 1632–1644.

Cloutier, M., Germain, M., Laliberté, E., 2023. Quebec trees dataset. Zenodo. https://doi.org/10.5281/zenodo.8148479.

Costanza, L., Lorente, B., Pedrero Salcedo, F., Pasanisi, F., Giannico, V., Ardito, F., Martí Martínez, C.M., Garofalo, S.P., 2025. Predicting olive tree chlorophyll fluorescence using explainable AI with sentinel-2 imagery in Mediterranean environment. Applied Sciences 15 (5), 2746.

Cui, X., Sun, M., Chen, Z., Li, M., Zhang, X., 2025. Deep learning-based urban tree species mapping with high-resolution pléiades imagery in Nanjing, china. Forests 16 (5), 783.

De Lima, R.A.F., Phillips, O.L., Duque, A., Tello, J.S., Davies, S.J., De Oliveira, A.A., Muller, S., Honorio Coronado, E.N., Vilanova, E., Cuni-Sanchez, A., Baker, T.R., Ryan, C.M., Malizia, A., Lewis, S.L., Ter Steege, H., Ferreira, J., Marimon, B.S., Luu, H.T., Imani, G., Arroyo, L., Blundo, C., Kenfack, D., Sainge, M.N., Sonké, B., Vásquez, R., 2022. Making forest data fair and open. Nature Ecology & Evolution 6 (6), 656–658.

Desai, S., Ghose, D., 2022. Active learning for improved semi-supervised semantic segmentation in satellite images. Proc. 2022 IEEE/CVF Winter Conference on Applications of Computer Vision (WACV), IEEE, Waikoloa, HI, USA, January, pp. 1485–1495.

Diez, Y., Kentsch, S., Fukuda, M., Caceres, M.L.L., Moritake, K., Cabezas, M., 2021. Deep learning in forestry using UAV-acquired RGB data: a practical review. Remote Sensing 13 (14), 2837.

Dollinger, J., Brun, P., Sainte Fare Garnot, V., Wegner, J.D., 2024. Sat-SINR: high-resolution species distribution models through satellite imagery. ISPRS Annals of the Photogrammetry, Remote Sensing and Spatial Information Sciences X-2–2024, 41–48.

Dosovitskiy, A., Beyer, L., Kolesnikov, A., Weissenborn, D., Zhai, X., Unterthiner, T., Dehghani, M., Minderer, M., Heigold, G., Gelly, S., Uszkoreit, J., Houlsby, N., 2020. An image is worth 16x16 words: transformers for image recognition at scale. arXiv:2010.11929.

Dubrovin, I., Fortin, C., Kedrov, A., 2024. An open dataset for individual tree detection in UAV LiDAR point clouds and RGB orthophotos in dense mixed forests. Scientific Reports 14 (1), 21938.

Ecke, S., Stehr, F., Frey, J., Tiede, D., Dempewolf, J., Klemmt, H.-J., Endres, E., Seifert, T., 2024. Towards operational UAV-based forest health monitoring: species identification and crown condition assessment by means of deep learning. Computers and Electronics in Agriculture 219, 108785.

Egli, S., Höpke, M., 2020. CNN-based tree species classification using high resolution RGB image data from automated UAV observations. Remote Sensing 12 (23), 3892.

Endres, J., Laliberté, E., Rolnick, D., Ouaknine, A., 2026. Estimating individual tree height and species from UAV imagery. arXiv:2603.23669.

European commission, 2026. Forest strategy for 2030, https://environment.ec.europa.eu/strategy/forest-strategy_en. (Accessed 11 December, 2025).

FAO, 2022. Global ecological zones (second edition), https://data.apps.fao.org/catalog/dataset/2fb209d0-fd34-4e5e-a3d8-a13c241eb61b. (Accessed 4 December, 2025).

FAO and UNEP, 2020. The state of the world's forests 2020, FAO and UNEP.

Fassnacht, F.E., Latifi, H., Stereńczak, K., Modzelewska, A., Lefsky, M., Waser, L.T., Straub, C., Ghosh, A., 2016. Review of studies on tree species classification from remotely sensed data. Remote Sensing of Environment 186, 64–87.

Fassnacht, F.E., White, J.C., Wulder, M.A., Næsset, E., 2024. Remote sensing in forestry: current challenges, considerations and directions. Forestry: an International Journal of Forest Research 97 (1), 11–37.

Féret, J.-B., Gitelson, A.A., Noble, S.D., Jacquemoud, S., 2017. PROSPECT-D: towards modeling leaf optical properties through a complete lifecycle. Remote Sensing of Environment 193, 204–215.

Ferreira, M.P., Almeida, D.R.A.D., Papa, D.D.A., Minervino, J.B.S., Veras, H.F.P., Formighieri, A., Santos, C.A.N., Ferreira, M.A.D., Figueiredo, E.O., Ferreira, E.J.L., 2020. Individual tree detection and species classification of amazonian palms using UAV images and deep learning. Forest Ecology and Management 475, 118397.

Ferreira, M.P., Dos Santos, D.R., Ferrari, F., Coelho, L.C.T., Martins, G.B., Feitosa, R.Q., 2024. Improving urban tree species classification by deep-learning based fusion of digital aerial images and LiDAR. Urban Forestry & Urban Greening 94, 128240.

Ferreira, M.P., Dos Santos, D.R., Ferrari, F., Martins, G.B., Feitosa, R.Q., 2023. Combining lidar-derived metrics with rgb-nir images to improve tree species classification in a tropical urban area. IGARSS 2023 - 2023 IEEE International Geoscience and Remote Sensing Symposium, IEEE, Pasadena, CA, USA, 16 July, pp. 5914–5917.

Ferreira, M.P., Lotte, R.G., D'Elia, F.V., Stamatopoulos, C., Kim, D.-H., Benjamin, A.R., 2021. Accurate mapping of Brazil nut trees (bertholletia excelsa) in amazonian forests using WorldView-3 satellite images and convolutional neural networks. Ecological Informatics 63, 101302.

Fournier, R.A., Edwards, G., Eldridge, N.R., 1995. A catalogue of potential spatial discriminators for high spatial resolution digital images of individual crowns. Canadian Journal of Remote Sensing 21 (3), 285–298.

Fu, M., Lu, C., Mao, Y., Zhang, X., Wu, Y., Luo, H., Liu, Z., Li, W., Ou, G., 2024. An efficient and accurate deep learning method for tree species classification that integrates depthwise separable convolution and dilated convolution using hyperspectral data. International Journal of Digital Earth 17 (1), 2307999.

Galdames, F., González, P., Magni-Pérez, F., Funk, S.M., Lepín, F., Saavedra, R., Hernández, H.J., 2023. Classification of trees in hyperspectral canopy data using machine learning: comparative analysis of forest structure complexity. The International Archives of the Photogrammetry, Remote Sensing and Spatial Information Sciences XLVIII-1/W2-2023, 1737–1742.

GBIF Secretariat, 2023. GBIF backbone taxonomy, https://www.gbif.org/dataset/d7dddbf4-2cf0-4f39-9b2a-bb099caae36c. (Accessed 4 December, 2025).

Gessler, A., Schaub, M., Bose, A., Trotsiuk, V., Valbuena, R., Chirici, G., Buchmann, N., 2024. Finding the balance between open access to forest data while safeguarding the integrity of national forest inventory-derived information. New Phytologist 242 (2), 344–346.

Ghassemian, H., 2016. A review of remote sensing image fusion methods. Information Fusion 32, 75–89.

Gibril, M.B.A., Shafri, H.Z.M., Shanableh, A., Al-Ruzouq, R., Wayayok, A., Hashim, S.J., 2021. Deep convolutional neural network for large-scale date palm tree mapping from UAV-based images. Remote Sensing 13 (14), 2787.

Gong, Yuhong, Wang, N., Wang, A., Zhang, Y., 2025. Tree species classification in UAV images based on domain-invariant features and generalized long-tail distribution. Journal of Applied Remote Sensing 19 (3), 038502.

Gong, Yulin, Zhu, D., Li, X., Lv, L., Zhang, B., Xuan, J., Du, H., 2024. Using UAV LiDAR intensity frequency and hyperspectral features to improve the accuracy of urban tree species classification. IEEE Journal of Selected Topics in Applied Earth Observations and Remote Sensing 17, 2849–2865.

Gougeon, F.A., 1995. A crown-following approach to the automatic delineation of individual tree crowns in high spatial resolution aerial images. Canadian Journal of Remote Sensing 21 (3), 274–284.

Grabska, E., Frantz, D., Ostapowicz, K., 2020. Evaluation of machine learning algorithms for forest stand species mapping using sentinel-2 imagery and environmental data in the polish carpathians. Remote Sensing of Environment 251, 112103.

Guo, Xianfei, Li, H., Jing, L., Wang, P., 2022. Individual tree species classification based on convolutional neural networks and multitemporal high-resolution remote sensing images. Sensors 22 (9), 3157.

Guo, Xuzhan, Liu, Q., Sharma, R.P., Chen, Q., Ye, Q., Tang, S., Fu, L., 2021. Tree recognition on the plantation using UAV images with ultrahigh spatial resolution in a complex environment. Remote Sensing 13 (20), 4122.

Hajjaji, Y., Boulila, W., Farah, I.R., 2022. Leveraging artificial intelligence techniques for smart palm tree detection: a decade systematic review. Procedia Computer Science 207, 2823–2832.

Hamedianfar, A., Mohamedou, C., Kangas, A., Vauhkonen, J., 2022. Deep learning for forest inventory and planning: a critical review on the remote sensing approaches so far and prospects for further applications. Forestry: an International Journal of Forest Research 95 (4), 451–465.

Hartling, S., Sagan, V., Sidike, P., Maimaitijiang, M., Carron, J., 2019. Urban tree species classification using a WorldView-2/3 and LiDAR data fusion approach and deep learning. Sensors 19 (6), 1284.

Hassija, V., Chamola, V., Mahapatra, A., Singal, A., Goel, D., Huang, K., Scardapane, S., Spinelli, I., Mahmud, M., Hussain, A., 2024. Interpreting black-box models: a review on explainable artificial intelligence. Cognitive Computation 16 (1), 45–74.

Hauser, S., Augner, L., Schmitt, A., 2025. Perfect labelling: a review and outlook of label optimization techniques in dynamic earth observation. Remote Sensing 17 (7), 1246.

He, K., Gkioxari, G., Dollar, P., Girshick, R., 2017. Mask R-CNN. Proc. Proceedings of the IEEE International Conference on Computer Vision, pp. 2961–2969.

He, R., Liu, L., Ye, H., Tan, Q., Ding, B., Cheng, L., Low, J., Bing, L., Si, L., 2021. On the effectiveness of adapter-based tuning for pretrained language model adaptation. Proc. Proceedings of the 59th Annual Meeting of the Association for Computational Linguistics and the 11th International Joint Conference on Natural Language Processing (Volume 1: Long Papers), Association for Computational Linguistics, Online, pp. 2208–2222.

He, Z., He, D., 2021. Bilinear squeeze-and-excitation network for fine-grained classification of tree species. IEEE Geoscience and Remote Sensing Letters 18 (7), 1139–1143.

Hiernaux, P., Issoufou, H.B.-A., Igel, C., Kariryaa, A., Kourouma, M., Chave, J., Mougin, E., Savadogo, P., 2023. Allometric equations to estimate the dry mass of sahel woody plants mapped with very-high resolution satellite imagery. Forest Ecology and Management 529, 120653.

Hou, B., Lin, C., Chen, M., Gouda, M.M., Zhao, Y., Chen, Y., Liu, F., Feng, X., 2025. Integrating UAV-based RGB imagery with semi-supervised learning for tree species identification in heterogeneous forests. Remote Sensing 17 (15), 2541.

Hou, C., Liu, Z., Chen, Y., Wang, S., Liu, A., 2023. Tree species classification from airborne hyperspectral images using spatial–spectral network. Remote Sensing 15 (24), 5679.

Hu, E.J., Shen, Y., Wallis, P., Allen-Zhu, Z., Li, Y., Wang, S., Wang, L., Chen, W., 2021. LoRA: low-rank adaptation of large language models. .

Huang, Y., Wen, X., Gao, Y., Zhang, Y., Lin, G., 2023. Tree species classification in UAV remote sensing images based on super-resolution reconstruction and deep learning. Remote Sensing 15 (11), 2942.

Imangholiloo, M., Luoma, V., Holopainen, M., Vastaranta, M., Mäkeläinen, A., Koivumäki, N., Honkavaara, E., Khoramshahi, E., 2023. A new approach for feeding multispectral imagery into convolutional neural networks improved classification of seedlings. Remote Sensing 15 (21), 5233.

Jacquemoud, S., Verhoef, W., Baret, F., Bacour, C., Zarco-Tejada, P.J., Asner, G.P., François, C., Ustin, S.L., 2009. PROSPECT+SAIL models: a review of use for vegetation characterization. Remote Sensing of Environment 113, S56–S66.

Johnson, J.M., Khoshgoftaar, T.M., 2019. Survey on deep learning with class imbalance. Journal of Big DATA 6 (1), 27.

Kattenborn, T., Leitloff, J., Schiefer, F., Hinz, S., 2021. Review on convolutional neural networks (CNN) in vegetation remote sensing. ISPRS Journal of Photogrammetry and Remote Sensing 173, 24–49.

Kattenborn, T., Lopatin, J., Förster, M., Braun, A.C., Fassnacht, F.E., 2019. UAV data as alternative to field sampling to map woody invasive species based on combined sentinel-1 and sentinel-2 data. Remote Sensing of Environment 227, 61–73.

Kattenborn, T., Schiefer, F., Frey, J., Feilhauer, H., Mahecha, M.D., Dormann, C.F., 2022. Spatially autocorrelated training and validation samples inflate performance assessment of convolutional neural networks. ISPRS Open Journal of Photogrammetry and Remote Sensing 5, 100018.

Kilian, G., Janusch, V.-J., Daniel, L., Björn, G., Teja, K., Maximilian, S., 2026. 3Dtrees.earth: technical infrastructure for FAIR forest LiDAR data management and analysis. 46. Wissenschaftlich-Technische Jahrestagung Der DGPF , 2527. März 2026 in Darmstadt; 321.

Klimadatastyrelsen, Dataforsyningen - din indgang til frie offentlige geodata og kort, https://dataforsyningen.dk/. (Accessed 11 December, 2025).

Korznikov, K., Kislov, D., Petrenko, T., Dzizyurova, V., Doležal, J., Krestov, P., Altman, J., 2023. Unveiling the potential of drone-borne optical imagery in forest ecology: a study on the recognition and mapping of two evergreen coniferous species. Remote Sensing 15 (18), 4394.

La Rosa, L.E.C., Sothe, C., Feitosa, R.Q., De Almeida, C.M., Schimalski, M.B., Oliveira, D.A.B., 2021. Multi-task fully convolutional network for tree species mapping in dense forests using small training hyperspectral data. ISPRS Journal of Photogrammetry and Remote Sensing 179, 35–49.

Lassalle, G., Ferreira, M.P., Cué La Rosa, L.E., Del'Papa Moreira Scafutto, R., De Souza Filho, C.R., 2023. Advances in multi- and hyperspectral remote sensing of mangrove species: a synthesis and study case on airborne and multisource spaceborne imagery. ISPRS Journal of Photogrammetry and Remote Sensing 195, 298–312.

LeCun, Y., Bengio, Y., Hinton, G., 2015. Deep learning. Nature 521 (7553), 436–444.

Lee, S.S., Lim, L.G., Palaiahnakote, S., Cheong, J.X., Lock, S.S.M., Ayub, M.N.B., 2024. Oil palm tree detection in UAV imagery using an enhanced RetinaNet. Computers and Electronics in Agriculture 227, 109530.

Lei, Z., Li, H., Zhao, J., Jing, L., Tang, Y., Wang, H., 2022. Individual tree species classification based on a hierarchical convolutional neural network and multitemporal google earth images. Remote Sensing 14 (20), 5124.

Lepcha, D.C., Goyal, B., Dogra, A., Goyal, V., 2023. Image super-resolution: a comprehensive review, recent trends, challenges and applications. Information Fusion 91, 230–260.

Li, W., Dong, R., Fu, H., Yu, L., 2018. Large-scale oil palm tree detection from high-resolution satellite images using two-stage convolutional neural networks. Remote Sensing 11 (1), 11–30.

Li, Y., Chai, G., Wang, Y., Lei, L., Zhang, X., 2022. ACE R-CNN: an attention complementary and edge detection-based instance segmentation algorithm for individual tree species identification using UAV RGB images and LiDAR data. Remote Sensing 14 (13), 3035.

Liang, X., Chen, J., Gong, W., Puttonen, E., Wang, Y., 2025. Influence of data and methods on high-resolution imagery-based tree species recognition considering phenology: the case of temperate forests. Remote Sensing of Environment 323, 114654.

Lin, C.-W., Ding, Q., Tu, W.-H., Huang, J.-H., Liu, J.-F., 2019. Fourier dense network to conduct plant classification using UAV-based optical images. IEEE Access 7, 17736–17749.

Lines, E.R., Allen, M., Cabo, C., Calders, K., Debus, A., Grieve, S.W.D., Miltiadou, M., Noach, A., Owen, H.J.F., Puliti, S., 2022. AI applications in forest monitoring need remote sensing benchmark datasets. arXiv:2212.09937.

Liu, F., Chen, D., Guan, Z., Zhou, X., Zhu, J., Ye, Q., Fu, L., Zhou, J., 2024. RemoteCLIP: a vision language foundation model for remote sensing. IEEE Transactions on Geoscience and Remote Sensing 62, 1–16.

Liu, S., Li, X., Zhen, Z., Zhao, Y., 2026. Switcher-HNet: a switchable hierarchical network for tree species classification from forest stand to individual tree tasks. ISPRS Journal of Photogrammetry and Remote Sensing 231, 329–344.

Liu, X., Gao, L., Jia, C., Cai, Y., Wang, G., Tian, Y., 2025. Classification of broad-leaved forest tree species based on HSFC-DeepLabV3+ in UAV multispectral images. IEEE Access 13, 174517–174534.

Lu, W., Niu, C., Lan, C., Liu, W., Wang, S., Yu, J., Hu, T., 2023. High-quality object detection method for UAV images based on improved DINO and masked image modeling. Remote Sensing 15 (19), 4740.

Ma, Y., Zhao, Y., Im, J., Zhao, Y., Zhen, Z., 2024. A deep-learning-based tree species classification for natural secondary forests using unmanned aerial vehicle hyperspectral images and LiDAR. Ecological Indicators 159, 111608.

Mao, Z., Abdi, O., Uusitalo, J., Laamanen, V., Kivinen, V.-P., 2025. Super-resolution supporting individual tree detection and canopy stratification using half-meter aerial data. ISPRS Journal of Photogrammetry and Remote Sensing 224, 251–271.

Martins, G.B., La Rosa, L.E.C., Happ, P.N., Coelho, L.C.T., Santos, C.J.F., Feitosa, R.Q., Ferreira, M.P., 2021. Deep learning-based tree species mapping in a highly diverse tropical urban setting. Urban Forestry & Urban Greening 64, 127241.

Mäyrä, J., Keski-Saari, S., Kivinen, S., Tanhuanpää, T., Hurskainen, P., Kullberg, P., Poikolainen, L., Viinikka, A., Tuominen, S., Kumpula, T., Vihervaara, P., 2021. Tree species classification from airborne hyperspectral and LiDAR data using 3D convolutional neural networks. Remote Sensing of Environment 256, 112322.

Mei, S., Lian, J., Wang, X., Su, Y., Ma, M., Chau, L.-P., 2024. A comprehensive study on the robustness of deep learning-based image classification and object detection in remote sensing: surveying and benchmarking. Journal of Remote Sensing 4, 0219.

Mellor, A., Boukir, S., Haywood, A., Jones, S., 2015. Exploring issues of training data imbalance and mislabelling on random forest performance for large area land cover classification using the ensemble margin. ISPRS Journal of Photogrammetry and Remote Sensing 105, 155–168.

Miao, S., Zhang, K. (Frank), Zeng, H., Liu, J., 2024. Improving artificial-intelligence-based individual tree species classification using pseudo tree crown derived from unmanned aerial vehicle imagery. Remote Sensing 16 (11), 1849.

Miyoshi, G.T., Arruda, M.D.S., Osco, L.P., Marcato Junior, J., Gonçalves, D.N., Imai, N.N., Tommaselli, A.M.G., Honkavaara, E., Gonçalves, W.N., 2020. A novel deep learning method to identify single tree species in UAV-based hyperspectral images. Remote Sensing 12 (8), 1294.

Mosig, C., Vajna-Jehle, J., Mahecha, M.D., Cheng, Y., Hartmann, H., Montero, D., Junttila, S., Horion, S., Schwenke, M.B., Koontz, M.J., Maulud, K.N.A., Adu-Bredu, S., Al-Halbouni, D., Ali, M., Allen, M., Altman, J., Amorós, L., Angiolini, C., Astrup, R., Awada, H., Barrasso, C., Bartholomeus, H., Beck, P.S.A., Bozzini, A., Braun-Wimmer, J., Brede, B., Breunig, F.M., Brugnaro, S., Buras, A., Burchard-Levine, V., Camarero, J.J., Candotti, A., Capuder, L., Carrieri, E., Centritto, M., Chirici, G., Cloutier, M., Conciani, D., Cushman, K., Dalling, J.W., Dao, P.D., Dempewolf, J., Denter, M., Dogotari, M., Díaz-Delgado, R., Ecke, S., Eichel, J., Eltner, A., Fabbri, A., Fabi, M., Fassnacht, F., Ferreira, M.P., Fischer, F.J., Frey, J., Frick, A., Fuentes, J., Ganz, S., Garbarino, M., García, M., Gassilloud, M., Gazol, A., Gea-Izquierdo, G., Gerberding, K., Ghasemi, M.,

Giannetti, F., Gillan, J., Gonzalez, R., Gosper, C., Greene, T., Greinwald, K., Grieve, S., Große-Stoltenberg, A., Gutierrez, J.A., Göritz, A., Hajek, P., Hedding, D., Hempel, J., Heremans, S., Hernández, M., Heurich, M., Honkavaara, E., Höfle, B., Jackisch, R., Jucker, T., Kalwij, J.M., Kepfer-Rojas, S., Khatri-Chhetri, P., Kleinebecker, T., Klemmt, H.-J., Klouček, T., Koivumäki, N., Kolagani, N., Komárek, J., Korznikov, K., Kraszewski, B., Kruse, S., Krüger, R., Kuechly, H., Kwong, I.H.Y., Laliberté, E., et al., 2026. deadtrees.earth — an open-access and interactive database for centimeter-scale aerial imagery to uncover global tree mortality dynamics. Remote Sensing of Environment 332, 115027.

Muhtar, D., Zhang, X., Xiao, P., Li, Z., Gu, F., 2023. CMID: a unified self-supervised learning framework for remote sensing image understanding. IEEE Transactions on Geoscience and Remote Sensing 61, 1–17.

Mustafa, Y.T., Habeeb, H.N., 2014. Object based technique for delineating and mapping 15 tree species using VHR WorldView-2 imagery. In: Neale, C.M.U., Maltese, A. (Eds), Remote Sensing for Agriculture, Ecosystems, and Hydrology XVI, SPIE, Amsterdam, Netherlands, 29 October, pp. 92390G.

Nagendra, H., 2001. Using remote sensing to assess biodiversity. International Journal of Remote Sensing 22 (12), 2377–2400.

Nezami, S., Khoramshahi, E., Nevalainen, O., Pölönen, I., Honkavaara, E., 2020. Tree species classification of drone hyperspectral and RGB imagery with deep learning convolutional neural networks. Remote Sensing 12 (7), 1070.

Olariu, H.G., Malambo, L., Popescu, S.C., Virgil, C., Wilcox, B.P., 2022. Woody plant encroachment: evaluating methodologies for semiarid woody species classification from drone images. Remote Sensing 14 (7), 1665.

Olsson, M., 2024. Early detection of bark beetle attacks: integrating segment anything model (SAM) zero-shot segmentation and spectral indices for tree health assessment. Student Thesis Series INES , 1–56.

Onishi, M., Ise, T., 2021. Explainable identification and mapping of trees using UAV RGB image and deep learning. Scientific Reports 11 (1), 903–917.

Onishi, M., Watanabe, S., Nakashima, T., Ise, T., 2022. Practicality and robustness of tree species identification using UAV RGB image and deep learning in temperate forest in Japan. Remote Sensing 14 (7), 1710.

Pal, O.K., Shovon, M.S.H., Mridha, M.F., Shin, J., 2024. In-depth review of AI-enabled unmanned aerial vehicles: trends, vision, and challenges. Discover Artificial Intelligence 4 (1), 97–120.

Pan, S.J., Yang, Q., 2010. A survey on transfer learning. IEEE Transactions on Knowledge and Data Engineering 22 (10), 1345–1359.

Parisi, G.I., Kemker, R., Part, J.L., Kanan, C., Wermter, S., 2019. Continual lifelong learning with neural networks: a review. Neural Networks 113, 54–71.

Pfadenhauer, J.S., Klötzli, F.A., 2020. Vegetation of the boreal (cold–temperate) zone. In: Pfadenhauer, J.S., Klötzli, F.A. (Eds), Global vegetation: fundamentals, ecology and distribution, Springer International Publishing, Cham, pp. 755–812.

Ploton, P., Mortier, F., Réjou-Méchain, M., Barbier, N., Picard, N., Rossi, V., Dormann, C., Cornu, G., Viennois, G., Bayol, N., Lyapustin, A., Gourlet-Fleury, S., Pélissier, R., 2020. Spatial validation reveals poor predictive performance of large-scale ecological mapping models. Nature Communications 11 (1), 4540.

Pohl, C., Van Genderen, J.L., 1998. Review article multisensor image fusion in remote sensing: concepts, methods and applications. International Journal of Remote Sensing 19 (5), 823–854.

Pu, R., 2021. Mapping tree species using advanced remote sensing technologies: a state-of-the-art review and perspective. Journal of Remote Sensing 2021, 2021/9812624.

Puliti, S., Lines, E.R., Müllerová, J., Frey, J., Schindler, Z., Straker, A., Allen, M.J., Winiwarter, L., Rehush, N., Hristova, H., Murray, B., Calders, K., Coops, N., Höfle, B., Irwin, L., Junttila, S., Krůček, M., Krok, G., Král, K., Levick, S.R., Luck, L., Missarov, A., Mokroš, M., Owen, H.J.F., Stereńczak, K., Pitkänen, T.P., Puletti, N., Saarinen, N., Hopkinson, C., Terryn, L., Torresan, C., Tomelleri, E., Weiser, H., Astrup, R., 2025. Benchmarking tree species classification from proximally sensed laser scanning data: introducing the FOR - SPECIES20K dataset. Methods in Ecology and Evolution 16 (4), 801–818.

Que, H., Gao, H., Shan, W., Liu, M., An, J., Deng, F., Feng, S., Yang, X., Mu, L., 2026. FM-SAM: individual tree crown delineation and classification based on segmentation anything model (SAM) and YOLOv10 in UAV imagery for forest monitoring. Computers and Electronics in Agriculture 240, 111162.

Radočaj, D., Jurišić, M., Gašparović, M., 2022. The role of remote sensing data and methods in a modern approach to fertilization in precision agriculture. Remote Sensing 14 (3), 778.

Roberts, D.R., Bahn, V., Ciuti, S., Boyce, M.S., Elith, J., Guillera-Arroita, G., Hauenstein, S., Lahoz-Monfort, J.J., Schröder, B., Thuiller, W., Warton, D.I., Wintle, B.A., Hartig, F., Dormann, C.F., 2017. Cross-validation strategies for data with temporal, spatial, hierarchical, or phylogenetic structure. Ecography 40 (8), 913–929.

Rumelhart, D.E., Hinton, G.E., Williams, R.J., 1986. Learning representations by back-propagating errors. Nature 323 (6088), 533–536.

Russell, D., Weinstein, B., Wettergreen, D., Young, D., 2024. Classifying geospatial objects from multiview aerial imagery using semantic meshes. arXiv:2405.09544.

Santos, A.A.D., Marcato Junior, J., Araújo, M.S., Di Martini, D.R., Tetila, E.C., Siqueira, H.L., Aoki, C., Eltner, A., Matsubara, E.T., Pistori, H., Feitosa, R.Q., Liesenberg, V., Gonçalves, W.N., 2019. Assessment of CNN-based methods for individual tree detection on images captured by RGB cameras attached to UAVs. Sensors 19 (16), 3595.

Schiefer, F., Kattenborn, T., Frick, A., Frey, J., Schall, P., Koch, B., Schmidtlein, S., 2020. Mapping forest tree species in high resolution UAV-based RGB-imagery by means of convolutional neural networks. ISPRS Journal of Photogrammetry and Remote Sensing 170, 205–215.

Shanin, V., Komarov, A., Mäkipää, R., 2014. Tree species composition affects productivity and carbon dynamics of different site types in boreal forests. European Journal of Forest Research 133 (2), 273–286.

Simmler, N., Sager, P., Andermatt, P., Chavarriaga, R., Schilling, F.-P., Rosenthal, M., Stadelmann, T., 2021. A survey of un-, weakly-, and semi-supervised learning methods for noisy, missing and partial labels in industrial vision applications. 2021 8th Swiss Conference on Data Science (SDS), IEEE, Lucerne, Switzerland, June, pp. 26–31.

Sivanandam, P., Lucieer, A., 2022. Tree detection and species classification in a mixed species forest using unoccupied aircraft system (UAS) RGB and multispectral imagery. Remote Sensing 14 (19), 4963.

Sobhana, M., Vardhan, J.A., Sravanthi, P.S., Santosh Reddy, K.U., 2025. Deep learning-based multi-angle classification of tree species from UAV images. Proc. 2025 IEEE International Conference on Recent Advances in Computing and Systems (REACS), IEEE, Gwalior, India, 19 December, pp. 1–6.

Soltani, S., Feilhauer, H., Duker, R., Kattenborn, T., 2022. Transfer learning from citizen science photographs enables plant species identification in UAV imagery. ISPRS Open Journal of Photogrammetry and Remote Sensing 5, 100016.

Soltani, S., Ferlian, O., Eisenhauer, N., Feilhauer, H., Kattenborn, T., 2024. From simple labels to semantic image segmentation: leveraging citizen science plant photographs for tree species mapping in drone imagery. Biogeosciences 21 (11), 2909–2935.

Sothe, C., De Almeida, C.M., Schimalski, M.B., La Rosa, L.E.C., Castro, J.D.B., Feitosa, R.Q., Dalponte, M., Lima, C.L., Liesenberg, V., Miyoshi, G.T., Tommaselli, A.M.G., 2020. Comparative performance of convolutional neural network, weighted and conventional support vector machine and random forest for classifying tree species using hyperspectral and photogrammetric data. GIScience & Remote Sensing 57 (3), 369–394.

Sun, M., Debulois, S.G.P., Zhang, Z., Cui, X., Chen, Z., Li, M., 2025. An improved hybrid approach involving deep learning for urban greening tree species classification with pléiades neo 4 imagery—a case study from Nanjing, eastern China. Ecological Informatics 90, 103331.

Sun, Y., Xin, Q., Huang, J., Huang, B., Zhang, H., 2019. Characterizing tree species of a tropical wetland in southern China at the individual tree level based on convolutional neural network. IEEE Journal of Selected Topics in Applied Earth Observations and Remote Sensing 12 (11), 4415–4425.

Sun, Z., Xue, B., Zhang, M., Schindler, J., 2025. YOLOv8E: an efficient YOLOv8 method for instance segmentation of individual tree crowns in Wellington city, new zealand. Journal of the Royal Society of New Zealand 55 (6), 1854–1879.

Swissimage, https://www.swisstopo.admin.ch/de/orthobilder-swissimage-10-cm. (Accessed 11 December, 2025).

Szwarcman, D., Roy, S., Fraccaro, P., Gíslason, Þ.E., Blumenstiel, B., Ghosal, R., De Oliveira, P.H., De Sousa Almeida, J.L., Sedona, R., Kang, Y., Chakraborty, S., Wang, S., Gomes, C., Kumar, A., Gaur, V., Truong, M., Godwin, D., Khallaghi, S., Lee, H., Hsu, C.-Y., Asanjan, A.A., Mujeci, B., Shidham, D., Balogun, R.O., Kolluru, V., Keenan, T., Arevalo, P., Li, W., Alemohammad, H., Olofsson, P., Mayer, T., Hain, C., Kennedy, R., Zadrozny, B., Bell, D., Cavallaro, G., Watson, C., Maskey, M., Ramachandran, R., Moreno, J.B., 2026. Prithvi-EO-2.0: a versatile multitemporal foundation model for Earth observation applications. IEEE Transactions on Geoscience and Remote Sensing 64, 1–20.

Tagle Casapia, X., Cardenas-Vigo, R., Marcos, D., Fernández Gamarra, E., Bartholomeus, H., Honorio Coronado, E.N., Di Liberto Porles, S., Falen, L., Palacios, S., Tsenbazar, N.-E., Mitchell, G., Dávila Díaz, A., Draper, F.C., Flores Llampazo, G., Pérez-Peña, P., Chipana, G., Del Castillo Torres, D., Herold, M., Baker, T.R., 2025. Effective integration of drone technology for mapping and managing palm species in the peruvian amazon. Nature Communications 16 (1), 3764.

Taylor, A.R., Chen, H.Y.H., VanDamme, L., 2009. A review of forest succession models and their suitability for forest management planning. Forest Science 55 (1), 23–36.

Thapa, B., Darling, L., Choi, D.H., Ardohain, C.M., Firoze, A., Aliaga, D.G., Hardiman, B.S., Fei, S., 2024. Application of multi-temporal satellite imagery for urban tree species identification. Urban Forestry & Urban Greening 98, 128409.

Tong, K., Wu, Y., 2022. Deep learning-based detection from the perspective of small or tiny objects: a survey. Image and Vision Computing 123, 104471.

Tuia, D., Schindler, K., Demir, B., Zhu, X.X., Kochupillai, M., Džeroski, S., Van Rijn, J.N., Hoos, H.H., Frate, F.D., Datcu, M., Markl, V., Saux, B.L., Schneider, R., Camps-Valls, G., 2025. Artificial intelligence to advance earth observation: a review of models, recent trends, and pathways forward. IEEE Geoscience and Remote Sensing Magazine 13 (4), 119–141.

Van De Ven, G.M., Tuytelaars, T., Tolias, A.S., 2022. Three types of incremental learning. Nature Machine Intelligence 4 (12), 1185–1197.

Van Der Plas, F., Ratcliffe, S., Ruiz-Benito, P., Scherer-Lorenzen, M., Verheyen, K., Wirth, C., Zavala, M.A., Ampoorter, E., Baeten, L., Barbaro, L., Bastias, C.C., Bauhus, J., Benavides, R., Benneter, A., Bonal, D., Bouriaud, O., Bruelheide, H., Bussotti, F., Carnol, M., Castagneyrol, B., Charbonnier, Y., Cornelissen, J.H.C., Dahlgren, J., Checko, E., Coppi, A., Dawud, S.M., Deconchat, M., De Smedt, P., De Wandeler, H., Domisch, T., Finér, L., Fotelli, M., Gessler, A., Granier, A., Grossiord, C., Guyot, V., Haase, J., Hättenschwiler, S., Jactel, H., Jaroszewicz, B., Joly, F.-X., Jucker, T., Kambach, S., Kaendler, G., Kattge, J., Koricheva, J., Kunstler, G., Lehtonen, A., Liebergesell, M., Manning, P., Milligan, H., Müller, S., Muys, B., Nguyen, D., Nock, C., Ohse, B., Paquette, A., Peñuelas, J., Pollastrini, M., Radoglou, K., Raulund-Rasmussen, K., Roger, F., Seidl, R., Selvi, F., Stenlid, J., Valladares, F., Van Keer, J., Vesterdal, L., Fischer, M., Gamfeldt, L., Allan, E., 2018. Continental mapping of forest ecosystem functions reveals a high but unrealised potential for forest multifunctionality. Ecology Letters 21 (1), 31–42.

Vaswani, A., Shazeer, N., Parmar, N., Uszkoreit, J., Jones, L., Gomez, A.N., Kaiser, L., Polosukhin, I., 2017. Attention is all you need. arXiv:1706.03762.

Vaz, A.S., Alcaraz-Segura, D., Campos, J.C., Vicente, J.R., Honrado, J.P., 2018. Managing plant invasions through the lens of remote sensing: a review of progress and the way forward. Science of the Total Environment 642, 1328–1339.

Veras, H.F.P., Ferreira, M.P., Da Cunha Neto, E.M., Figueiredo, E.O., Corte, A.P.D., Sanquetta, C.R., 2022. Fusing multi-season UAS images with convolutional neural networks to map tree species in amazonian forests. Ecological Informatics 71, 101815.

Vu-Duc, A., Nguyen-Vi, K., Bui-Quoc, B., Kamel, N., 2025. A comprehensive survey of super-resolution remote sensing image datasets: evolution, challenges, and future directions. IEEE Access 13, 145350–145372.

Wang, L., Zhou, Y., Hu, Q., Tang, Z., Ge, Y., Smith, A., Awada, T., Shi, Y., 2021. Early detection of encroaching woody juniperus virginiana and its classification in multi-species forest using UAS imagery and semantic segmentation algorithms. Remote Sensing 13 (10), 1975.

Wang, P., Bayram, B., Sertel, E., 2022. A comprehensive review on deep learning based remote sensing image super-resolution methods. Earth-Science Reviews 232, 104110.

Wang, Q., Pu, Z., Luo, L., Wang, L., Gao, J., 2025. A study on tree species recognition in UAV remote sensing imagery based on an improved YOLOv11 model. Applied Sciences 15 (16), 8779.

Wang, X., Zhang, Y., Ca, J., Qin, Q., Feng, Y., Yan, J., 2024. Semantic segmentation network for mangrove tree species based on UAV remote sensing images. Scientific Reports 14 (1), 29860.

Wang, Z., Wu, Y., Niu, Q., 2020. Multi-sensor fusion in automated driving: a survey. IEEE Access 8, 2847–2868.

Weinstein, B., Marconi, S., Zare, A., Bohlman, S., Graves, S., Singh, A., White, E., 2020. NEON tree crowns dataset. Zenodo. https://doi.org/10.5281/zenodo.3765872.

Weinstein, B.G., Marconi, S., Aubry-Kientz, M., Vincent, G., Senyondo, H., White, E.P., 2020. DeepForest: a PYTHON package for RGB deep learning tree crown delineation. Methods in Ecology and Evolution 11 (12), 1743–1751.

Weinstein, B.G., Marconi, S., Bohlman, S.A., Zare, A., White, E.P., 2020. Cross-site learning in deep learning RGB tree crown detection. Ecological Informatics 56, 101061.

Weinstein, B.G., Marconi, S., Graves, S.J., Zare, A., Singh, A., Bohlman, S.A., Magee, L., Johnson, D.J., Townsend, P.A., White, E.P., 2023. Capturing long-tailed individual tree diversity using an airborne imaging and a multi-temporal hierarchical model. Remote Sensing in Ecology and Conservation 9 (5), 656–670.

Wu, Z., Bodla, N., Singh, B., Najibi, M., Chellappa, R., Davis, L.S., 2018. Soft sampling for robust object detection. arXiv:1806.06986.

Xiong, Z., Zhang, F., Wang, Y., Shi, Y., Zhu, X.X., 2025. EarthNets: empowering artificial intelligence for Earth observation. IEEE Geoscience and Remote Sensing Magazine 13 (4), 45–78.

Xu, L., Lu, C., Zhou, T., Wu, J., Feng, H., 2024. A 3D-2DCNN-CA approach for enhanced classification of hickory tree species using UAV-based hyperspectral imaging. Microchemical Journal 199, 109981.

Xu, M., Bai, Y., Ghanem, B., 2019. Missing labels in object detection. CVPR Workshops , 1–10.

Yan, S., Jing, L., Wang, H., 2021. A new individual tree species recognition method based on a convolutional neural network and high-spatial resolution remote sensing imagery. Remote Sensing 13 (3), 479–498.

Yao, H., Qin, R., Chen, X., 2019. Unmanned aerial vehicle for remote sensing applications—a review. Remote Sensing 11 (12), 1443.

Yao, Z., Chai, G., Lei, L., Jia, X., Zhang, X., 2023. Individual tree species identification and crown parameters extraction based on mask R-CNN: assessing the applicability of unmanned aerial vehicle optical images. Remote Sensing 15 (21), 5164.

Yun, T., Weng, G., Wang, R., Li, Y., Eichhorn, M.P., Zhang, H., 2026. LGINet: linguistic guided image diffusion model for tree species generation and identification from aerial imagery. Information Fusion 129, 103912.

Zhang, Che, Huang, Y., Sakharova, E.K., Kanev, A.I., Terekhov, V.I., 2023. TreeCurveNet - an improved CurveNet for tree species classification. In: Kryzhanovsky, B., Dunin-Barkowski, W., Redko, V., Tiumentsev, Y., Klimov, V. (Eds), Advances in neural computation, machine learning, and cognitive research VII, Springer Nature Switzerland, Cham, pp. 32–38.

Zhang, Chiyuan, Bengio, S., Hardt, M., Recht, B., Vinyals, O., 2016. Understanding deep learning requires rethinking generalization. arXiv:1611.03530.

Zhang, Chong, Zhou, J., Wang, H., Tan, T., Cui, M., Huang, Z., Wang, P., Zhang, L., 2022. Multi-species individual tree segmentation and identification based on improved mask R-CNN and UAV imagery in mixed forests. Remote Sensing 14 (4), 874–895.

Zhang, H., Chen, F., Shen, Z., Hao, Q., Zhu, C., Savvides, M., 2020. Solving missing-annotation object detection with background recalibration loss. ICASSP 2020 - 2020 IEEE International Conference on Acoustics, Speech and Signal Processing (ICASSP), IEEE, Barcelona, Spain, May, pp. 1888–1892.

Zhang, J., Lei, F., Fan, X., 2025. Parameter-efficient fine-tuning for individual tree crown detection and species classification using UAV-acquired imagery. Remote Sensing 17 (7), 1272.

Zhang, W., Wang, X., Wang, H., Cheng, Y., 2024. Causal meta-reinforcement learning for multimodal remote sensing data classification. Remote Sensing 16 (6), 1055.

Zhang, X., Gu, J., Azam, B., Zhang, W., Lin, M., Li, C., Jing, W., Akhtar, N., 2025. RSVMamba for tree species classification using UAV RGB remote sensing images. IEEE Transactions on Geoscience and Remote Sensing 63, 1–16.

Zhao, H., Morgenroth, J., Pearse, G., Schindler, J., 2023. A systematic review of individual tree crown detection and delineation with convolutional neural networks (CNN). Current Forestry Reports 9 (3), 149–170.

Zheng, J., Yuan, S., Li, W., Fu, H., Yu, L., Huang, J., 2025. A review of individual tree crown detection and delineation from optical remote sensing images: current progress and future. IEEE Geoscience and Remote Sensing Magazine 13 (1), 209–236.

Zhong, H., Zhang, Z., Liu, H., Wu, J., Lin, W., 2024. Individual tree species identification for complex coniferous and broad-leaved mixed forests based on deep learning combined with UAV LiDAR data and RGB images. Forests 15 (2), 293–312.

Zhu, X.X., Tuia, D., Mou, L., Xia, G.-S., Zhang, L., Xu, F., Fraundorfer, F., 2017. Deep learning in remote sensing: a comprehensive review and list of resources. IEEE Geoscience and Remote Sensing Magazine 5 (4), 8–36.

7. Acknowledgments

Z.X. and M.B. were supported by the Swiss National Science Foundation (SNSF) [grant number CRSII5_216562].

8. Author contributions

Z.X. and M.B.: Conceptualization, Visualization, Writing-original draft, Writing-review & editing. Z.X.: Investigation, Methodology, Data curation. T.K., J.D.W., A.G., and V.C.G.: Writing-review & editing

9. Competing interest

The authors declare no competing interests.

This is a non-peer-reviewed preprint submitted to EarthArXiv.

Supplementary information

Review of deep learning for tree species identification from high-resolution remote sensing imagery

Zhongyu Xia[1], Teja Kattenborn[2], Jan D. Wegner[3], Arthur Gessler[1,4], Verena C. Griess[1], Mirela Beloiu[1*]*

[1] Department of Environmental Systems Science, Institute of Terrestrial Ecosystems, ETH Zurich, 8092 Zurich, Switzerland
[2] Chair of Sensor-based Geoinformatics, University of Freiburg, 79106 Freiburg, Germany
[3] Department of Mathematical Modeling and Machine Learning, University of Zurich, Zurich, 8057, Switzerland
[4] Forest and Soil Ecology, Swiss Federal Institute for Forest, Snow and Landscape Research WSL, 8903 Birmensdorf, Switzerland
*Corresponding authors: Zhongyu Xia (zhongyu.xia@usys.ethz.ch) and Mirela Beloiu (mirela.beloiu@usys.ethz.ch)

Supplementary tables

Table S1. Relative difference analysis comparing additional spectral bands against RGB within each relevant reviewed study. Publication ID and Identification ID, correspond to them in the overall database in Table S6. Publication ID = Pub. ID and Identification ID = Identif. ID, Group ID = Gr. ID. Relative and absolute performance differences were calculated using either overall accuracy or F1-score, depending on data availability. For each paired comparison, the same metric was used for both model performances. Relative difference was calculated using Eq. 1 (Section 2.2 of Materials and Methods).

Pub. ID	Gr. No.	Identif. ID	Group	Data type	Overall accuracy	F1-score	Relative difference (%)	Absolute difference
4	1	13	Baseline	RGB	NA	0.19		
		7	Control group	Hyperspectral	NA	0.80	328.88%	0.62
		8	Control group	Hyperspectral	NA	0.79	320.32%	0.60
		9	Control group	Hyperspectral	NA	0.78	317.65%	0.59
		10	Control group	Hyperspectral	NA	0.76	303.74%	0.57
		11	Control group	Hyperspectral	NA	0.60	219.79%	0.41
		12	Control group	Hyperspectral	NA	0.67	257.75%	0.48
		14	Control group	Multispectral	NA	0.81	335.29%	0.63
		15	Control group	RGB-NIR	NA	0.76	304.81%	0.57
7	2	26	Baseline	RGB	0.97	NA		

This is a non-peer-reviewed preprint submitted to EarthArXiv.

Pub. ID	Gr. No.	Identif. ID	Group	Data type	Overall accuracy	F1-score	Relative difference (%)	Absolute difference
		25	Control group	Hyperspectral	0.97	NA	-0.10%	0.00
22	3	75	Baseline	RGB	NA	0.88		
		76	Control group	RGB-NIR	NA	0.88	0.00%	0.00
		77	Control group	Multispectral	NA	0.89	1.14%	0.01
	4	82	Baseline	RGB	NA	0.74		
		83	Control group	RGB-NIR	NA	0.73	-1.35%	-0.01
		84	Control group	Multispectral	NA	0.75	1.35%	0.01
	5	86	Baseline	RGB	NA	0.62		
		72	Control group	RGB-NIR	NA	0.64	3.23%	0.02
		73	Control group	Multispectral	NA	0.65	4.84%	0.03
	6	71	Baseline	RGB	NA	0.59		
		79	Control group	RGB-NIR	NA	0.58	-1.69%	-0.01
		80	Control group	Multispectral	NA	0.61	3.39%	0.02
28	7	162	Baseline	RGB	NA	0.64		
		161	Control group	Hyperspectral	NA	0.87	35.94%	0.23
64	8	336	Baseline	RGB	0.91	NA		
		340	Control group	Hyperspectral	0.99	NA	9.02%	0.08
	9	341	Baseline	RGB	0.73	NA		
		342	Control group	Hyperspectral	0.98	NA	34.78%	0.25
67	10	362	Baseline	RGB	0.95	NA		
		360	Control group	Multispectral	0.95	NA	0.42%	0.00
	11	366	Baseline	RGB	0.73	NA		
		364	Control group	Multispectral	0.73	NA	0.41%	0.00

Table S2. Relative difference analysis comparing multi-modal fusion against 2D single data source within each relevant reviewed study. Publication ID and Identification ID correspond to them in the overall database in Table S6. Publication ID = Pub. ID and Identification ID = Identif. ID, Group ID = Gr. ID. Relative and absolute performance differences were calculated using either overall accuracy or F1-score, depending on data availability. For each paired comparison, the same metric was used for both model performances. Relative difference was calculated using Eq. 1 (Section 2.2 of Materials and Methods).

Pub. ID	Gr. No.	Identif.ID	Group	Data type	Fusion strategy	Overall accuracy	F1-score	Relative difference (%)	Absolute difference
6	1	19	Baseline	2D		0.84	NA		
		20	Control group	2D + 3D	Early fusion	0.77	NA	-8.53%	-0.07
		21	Control group	2D + 3D	Early fusion	0.79	NA	-6.14%	-0.05
	2	22	Baseline	2D		0.75	NA		
		23	Control group	2D + 3D	Early fusion	0.70	NA	-6.12%	-0.05
		24	Control group	2D + 3D	Early fusion	0.73	NA	-2.44%	-0.02
7	3	26	Baseline	2D		0.97	NA		
		30	Control group	2D + 3D	Early fusion	0.98	NA	0.41%	0.00
	4	25	Baseline	2D		0.97	NA		
		28	Control group	2D + 3D	Early fusion	0.97	NA	-0.41%	0.00
		31	Control group	2D + 3D	Early fusion	0.98	NA	0.62%	0.01
		27	Control group	Other	Early fusion	0.98	NA	1.34%	0.01
		29	Control group	Other	Early fusion	0.97	NA	0.00%	0.00
22	5	77	Baseline	2D		NA	0.89		
		78	Control group	2D + 3D	Early fusion	NA	0.86	-3.37%	-0.03
	6	84	Baseline	2D		NA	0.75		
		85	Control group	2D + 3D	Early fusion	NA	0.70	-6.67%	-0.05
	7	73	Baseline	2D		NA	0.65		
		74	Control group	2D + 3D	Early fusion	NA	0.63	-3.08%	-0.02
	8	80	Baseline	2D		NA	0.61		
		81	Control group	2D + 3D	Early fusion	NA	0.56	-8.20%	-0.05
24	9	106	Baseline	2D		NA	0.72		
		107	Control group	Other	Early fusion	NA	0.68	-5.56%	-0.04
		108	Control group	Other	Early fusion	NA	0.78	8.33%	0.06
		109	Control group	Other	Early fusion	NA	0.76	5.56%	0.04

This is a non-peer-reviewed preprint submitted to EarthArXiv.

Pub. ID	Gr. No.	Identif.ID	Group	Data type	Fusion strategy	Overall accuracy	F1-score	Relative difference (%)	Absolute difference
	10	100	Baseline	2D		NA	0.66		
		101	Control group	Other	Early fusion	NA	0.61	-7.58%	-0.05
		102	Control group	Other	Early fusion	NA	0.72	9.09%	0.06
		103	Control group	Other	Early fusion	NA	0.74	12.12%	0.08
	11	112	Baseline	2D		NA	0.57		
		95	Control group	Other	Early fusion	NA	0.56	-1.75%	-0.01
		96	Control group	Other	Early fusion	NA	0.78	36.84%	0.21
		97	Control group	Other	Early fusion	NA	0.73	28.07%	0.16
34	12	193	Baseline	2D		NA	0.68		
		198	Control group	2D + 3D	Early fusion	NA	0.73	7.35%	0.05
	13	196	Baseline	2D		NA	0.69		
		200	Control group	2D + 3D	Early fusion	NA	0.67	-2.90%	-0.02
	14	196	Baseline	2D		NA	0.54		
		200	Control group	2D + 3D	Early fusion	NA	0.55	-2.90%	0.01
65	15	348	Baseline	2D		0.81	NA		
		351	Control group	Other	Early fusion	0.94	NA	16.43%	0.13
	16	346	Baseline	2D		0.71	NA		
		349	Control group	Other	Early fusion	0.82	NA	15.62%	0.11
	17	347	Baseline	2D		0.79	NA		
		350	Control group	Other	Early fusion	0.91	NA	15.49%	0.12
66	18	356	Baseline	2D		0.93	NA		
		359	Control group	Other	Early fusion	0.95	NA	2.09%	0.02
	19	354	Baseline	2D		0.85	NA		
		357	Control group	Other	Early fusion	0.89	NA	4.04%	0.03
	20	353	Baseline	2D		0.84	NA		
		358	Control group	Other	Early fusion	0.93	NA	10.14%	0.09
67	21	365	Baseline	2D		0.95	NA		
		362	Control group	Other		0.95	NA	-0.32%	0.00
		367	Control group	Other		0.95	NA	-0.21%	0.00
		369	Control group	Other		0.92	NA	-3.16%	-0.03
		371	Control group	Other		0.95	NA	-0.11%	0.00

This is a non-peer-reviewed preprint submitted to EarthArXiv.

Pub. ID	Gr. No.	Identif.ID	Group	Data type	Fusion strategy	Overall accuracy	F1-score	Relative difference (%)	Absolute difference
	22	366	Baseline	2D		0.73	NA		
		361	Control group	Other		0.69	NA	-4.69%	-0.03
		363	Control group	Other		0.73	NA	0.55%	0.00
		368	Control group	Other		0.73	NA	0.00%	0.00
		370	Control group	Other		0.68	NA	-6.07%	-0.04
88	23	386	Baseline	2D		0.61	NA		
		398	Control group	2D + 3D	Early fusion	0.71	NA	16.39%	0.10
		399	Control group	2D + 3D	Early fusion	0.75	NA	22.95%	0.14
	24	389	Baseline	2D		0.68	NA		
		390	Control group	2D + 3D	Early fusion	0.73	NA	7.35%	0.05
		391	Control group	2D + 3D	Early fusion	0.83	NA	22.06%	0.15
	25	387	Baseline	2D		0.61	NA		
		388	Control group	2D + 3D	Early fusion	0.68	NA	11.48%	0.07
		403	Control group	2D + 3D	Early fusion	0.56	NA	-8.20%	-0.05
	26	395	Baseline	2D		0.69	NA		
		396	Control group	2D + 3D	Early fusion	0.72	NA	4.35%	0.03
		397	Control group	2D + 3D	Early fusion	0.77	NA	11.59%	0.08
	27	392	Baseline	2D		0.66	NA		
		393	Control group	2D + 3D	Early fusion	0.68	NA	3.03%	0.02
		394	Control group	2D + 3D	Early fusion	0.73	NA	10.61%	0.07
	28	400	Baseline	2D		0.54	NA		
		401	Control group	2D + 3D	Early fusion	0.52	NA	-3.70%	-0.02
		402	Control group	2D + 3D	Early fusion	0.62	NA	14.81%	0.08
93	29	418	Baseline	2D		0.77	NA		
		419	Control group	2D + 3D	Middle fusion	0.78	NA	0.96%	0.01
		420	Control group	2D + 3D	Middle fusion	0.76	NA	-0.87%	-0.01
		421	Control group	2D + 3D	Middle fusion	0.78	NA	1.17%	0.01
		422	Control group	2D + 3D	Middle fusion	0.79	NA	2.44%	0.02
		423	Control group	2D + 3D	Middle fusion	0.77	NA	-0.14%	0.00
		424	Control group	2D + 3D	Middle fusion	0.70	NA	-9.02%	-0.07
		425	Control group	2D + 3D	Middle fusion	0.71	NA	-7.27%	-0.06

Pub. ID	Gr. No.	Identif.ID	Group	Data type	Fusion strategy	Overall accuracy	F1-score	Relative difference (%)	Absolute difference
94	30	426	Baseline	2D			0.83		
		427	Control group	2D + 3D	Middle fusion		0.99	18.19%	0.15
95	31	429	Baseline	2D		0.77	NA		
		430	Control group	2D + 3D	Early fusion	0.81	NA	5.61%	0.04
		431	Control group	2D + 3D	Early fusion	0.83	NA	7.57%	0.06
98	32	459	Baseline	2D		0.85	NA		
		456	Control group	2D + 3D	Early fusion	0.87	NA	2.36%	0.02
	33	455	Baseline	2D		0.86	NA		
		460	Control group	2D + 3D	Early fusion	0.91	NA	6.19%	0.05
	34	457	Baseline	2D		0.87	NA		
		461	Control group	2D + 3D	Early fusion	0.89	NA	2.30%	0.02
	35	458	Baseline	2D		0.83	NA		
		462	Control group	2D + 3D	Early fusion	0.89	NA	7.74%	0.06
102	36	475	Baseline	2D		NA	0.24		
		476	Control group	2D + 3D	Middle fusion	NA	0.40	69.49%	0.16
	37	473	Baseline	2D		NA	0.17		
		480	Control group	2D + 3D	Middle fusion	NA	0.50	190.75%	0.33
	38	484	Baseline	2D		NA	0.06		
		485	Control group	2D + 3D	Middle fusion	NA	0.26	344.07%	0.20
104	39	492	Baseline	2D		NA	0.73		
		495	Control group	2D + 3D	Early fusion	NA	0.74	1.64%	0.01
		496	Control group	2D + 3D	Early fusion	NA	0.75	2.19%	0.02
		497	Control group	2D + 3D	Early fusion	NA	0.76	4.37%	0.03
	40	501	Baseline	2D		NA	0.73		
		494	Control group	2D + 3D	Middle fusion	NA	0.73	0.14%	0.00
106	41	507	Baseline	2D		0.90			
		523	Control group	2D + 3D	Early fusion	0.87		-3.07%	-0.03
		525	Control group	Other	Early fusion	0.87		-2.77%	-0.02
108	42	546	Baseline	2D		NA	0.80		
		547	Control group	2D + 3D	Early fusion	NA	0.83	4.14%	0.03
		548	Control group	2D + 3D	Early fusion	NA	0.80	0.50%	0.00

This is a non-peer-reviewed preprint submitted to EarthArXiv.

Pub. ID	Gr. No.	Identif.ID	Group	Data type	Fusion strategy	Overall accuracy	F1-score	Relative difference (%)	Absolute difference
		549	Control group	2D + 3D	Early fusion	NA	0.79	-1.36%	-0.01
		550	Control group	2D + 3D	Early fusion	NA	0.81	1.04%	0.01
		551	Control group	2D + 3D	Early fusion	NA	0.77	-3.42%	-0.03
		552	Control group	2D + 3D	Early fusion	NA	0.76	-4.69%	-0.04
		553	Control group	2D + 3D	Early fusion	NA	0.76	-5.02%	-0.04
130	43	604	Baseline	2D		0.90	NA		
		605	Control group	Other	Early fusion	0.91	NA	0.91%	0.01
161	44	703	Baseline	2D		NA	0.52		
		704	Control group	Other		NA	0.54	3.63%	0.02
	45	699	Baseline	2D		NA	0.75		
		700	Control group	Other		NA	0.77	2.66%	0.02
	46	701	Baseline	2D		NA	0.71		
		702	Control group	Other		NA	0.69	-2.25%	-0.02
221	47	996	Baseline	2D		0.84	NA		
		997	Control group	2D + 3D	Early fusion	0.86	NA	1.58%	0.01
236	48	1016	Baseline	2D		NA	0.74		
		1017	Control group	2D + 3D	Early fusion	NA	0.72	-2.70%	-0.02
		1018	Control group	2D + 3D	Early fusion	NA	0.74	0.00%	0.00

Table S3. Relative difference analysis comparing multitemporal data against single temporal data within each relevant reviewed study. Publication ID and Identification ID correspond to them in the overall database in Table S6. Publication ID = Pub. ID and Identification ID = Identif. ID, Group ID = Gr. ID. Relative and absolute performance differences were calculated using either overall accuracy or F1-score, depending on data availability. For each paired comparison, the same metric was used for both model performances. Relative difference was calculated using Eq. 1 (Section 2.2 of Materials and Methods).

Pub. ID	Gr. No.	Identif. ID	Group	Temporality	Overall accuracy	F1-score	Relative difference (%)	Absolute difference
30	1	165	Baseline	Single-temporal	NA	0.50		
		164	Control group	Multi-temporal	NA	0.80	60.00%	0.30
35	2	204	Baseline	Single-temporal	0.83	NA		
		207	Control group	Multi-temporal	0.93	NA	11.69%	0.10
		208	Control group	Multi-temporal	0.89	NA	7.47%	0.06
		209	Control group	Multi-temporal	0.82	NA	-0.72%	-0.01
		210	Control group	Multi-temporal	0.80	NA	-3.49%	-0.03
	3	205	Baseline	Single-temporal	0.84	NA		
		207	Control group	Multi-temporal	0.93	NA	10.36%	0.09
		208	Control group	Multi-temporal	0.89	NA	6.19%	0.05
		209	Control group	Multi-temporal	0.82	NA	-1.90%	-0.02
		210	Control group	Multi-temporal	0.80	NA	-4.64%	-0.04
	4	206	Baseline	Single-temporal	0.84	NA		
		207	Control group	Multi-temporal	0.93	NA	10.36%	0.09
		208	Control group	Multi-temporal	0.89	NA	6.19%	0.05
		209	Control group	Multi-temporal	0.82	NA	-1.90%	-0.02
		210	Control group	Multi-temporal	0.80	NA	-4.64%	-0.04
51	5	268	Baseline	Single-temporal	0.59	NA		
		274	Control group	Multi-temporal	0.89	NA	51.49%	0.30
	6	271	Baseline	Single-temporal	0.77	NA		
		274	Control group	Multi-temporal	0.89	NA	15.64%	0.12
	7	280	Baseline	Single-temporal	0.78	NA		
		274	Control group	Multi-temporal	0.89	NA	14.99%	0.12
	8	283	Baseline	Single-temporal	0.68	NA		
		274	Control group	Multi-temporal	0.89	NA	32.02%	0.22

This is a non-peer-reviewed preprint submitted to EarthArXiv.

Pub. ID	Gr. No.	Identif. ID	Group	Temporality	Overall accuracy	F1-score	Relative difference (%)	Absolute difference
	9	286	Baseline	Single-temporal	0.63	NA		
		274	Control group	Multi-temporal	0.89	NA	41.92%	0.26
	10	267	Baseline	Single-temporal	0.55	NA		
		273	Control group	Multi-temporal	0.88	NA	59.74%	0.33
	11	270	Baseline	Single-temporal	0.71	NA		
		273	Control group	Multi-temporal	0.88	NA	24.79%	0.18
	12	276	Baseline	Single-temporal	0.73	NA		
		273	Control group	Multi-temporal	0.88	NA	21.46%	0.16
	13	282	Baseline	Single-temporal	0.70	NA		
		273	Control group	Multi-temporal	0.88	NA	25.84%	0.18
	14	285	Baseline	Single-temporal	0.59	NA		
		273	Control group	Multi-temporal	0.88	NA	50.51%	0.30
	15	266	Baseline	Single-temporal	0.54	NA		
		272	Control group	Multi-temporal	0.84	NA	55.43%	0.30
51	16	269	Baseline	Single-temporal	0.73	NA		
		272	Control group	Multi-temporal	0.84	NA	14.87%	0.11
	17	265	Baseline	Single-temporal	0.74	NA		
		272	Control group	Multi-temporal	0.84	NA	14.04%	0.10
	18	281	Baseline	Single-temporal	0.65	NA		
		272	Control group	Multi-temporal	0.84	NA	30.60%	0.20
	19	284	Baseline	Single-temporal	0.55	NA		
		272	Control group	Multi-temporal	0.84	NA	52.54%	0.29
53	20	291	Baseline	Single-temporal	NA	0.82		
		295	Control group	Multi-temporal	NA	0.90	10.04%	0.08
	21	292	Baseline	Single-temporal	NA	0.70		
		295	Control group	Multi-temporal	NA	0.90	27.70%	0.20
	22	293	Baseline	Single-temporal	NA	0.80		
		295	Control group	Multi-temporal	NA	0.90	12.09%	0.10
	23	294	Baseline	Single-temporal	NA	0.84		
		295	Control group	Multi-temporal	NA	0.90	6.52%	0.06
63	24	334	Baseline	Single-temporal	0.60	NA		

This is a non-peer-reviewed preprint submitted to EarthArXiv.

Pub. ID	Gr. No.	Identif. ID	Group	Temporality	Overall accuracy	F1-score	Relative difference (%)	Absolute difference
		335	Control group	Multi-temporal	0.75	NA	25.00%	0.15
196	25	836	Baseline	Single-temporal	0.81	NA		
		837	Control group	Multi-temporal	0.85	NA	4.38%	0.04
		838	Control group	Multi-temporal	0.85	NA	4.99%	0.04
		839	Control group	Multi-temporal	0.87	NA	7.22%	0.06
	26	860	Baseline	Single-temporal	0.58	NA		
		861	Control group	Multi-temporal	0.64	NA	9.75%	0.06
		862	Control group	Multi-temporal	0.65	NA	12.02%	0.07
		863	Control group	Multi-temporal	0.62	NA	6.48%	0.04
	27	844	Baseline	Single-temporal	0.75	NA		
		845	Control group	Multi-temporal	0.82	NA	9.80%	0.07
		846	Control group	Multi-temporal	0.82	NA	9.13%	0.07
		847	Control group	Multi-temporal	0.85	NA	13.55%	0.10
	28	852	Baseline	Single-temporal	0.65	NA		
		853	Control group	Multi-temporal	0.71	NA	10.04%	0.07
		854	Control group	Multi-temporal	0.69	NA	6.41%	0.04
		855	Control group	Multi-temporal	0.67	NA	3.13%	0.02

Table S4. Relative difference analysis comparing shallow machine learning approaches against deep learning approach within each relevant reviewed study. Publication ID, Identification ID, and shallow machine learning or deep learning models correspond to them in the overall database in Table S6. Publication ID = Pub. ID, Identification ID = Identif. ID, Group ID = Gr. ID., and ML/DL models = Shallow machine learning or deep learning models. Relative and absolute performance differences were calculated using either overall accuracy or F1-score, depending on data availability. For each paired comparison, the same metric was used for both model performances. Relative difference was calculated using Eq. 1 (Section 2.2 of Materials and Methods).

Pub. ID	Gr. No.	Identif. ID	ML/DL models	Overall accuracy	F1-score	Relative difference (%)	Absolute difference
2	1	3	Convolutional neural networks	0.76	NA		
		1060	Support vector machine	0.49	NA	-35.07%	-0.27
		1061	Random forest	0.47	NA	-37.44%	-0.28
3	2	4	Convolutional neural networks	NA	0.57		
		1062	Random forest	NA	0.38	-33.39%	-0.19
		1063	Support vector machine	NA	0.49	-12.79%	-0.07
	3	5	Convolutional neural networks	NA	0.76		
		1064	Random forest	NA	0.65	-14.53%	-0.11
		1065	Support vector machine	NA	0.73	-3.40%	-0.03
	4	6	Convolutional neural networks	NA	0.85		
		1066	Random forest	NA	0.66	-22.06%	-0.19
		1067	Support vector machine	NA	0.82	-3.38%	-0.03
6	5	22	Convolutional neural networks	0.75	NA		
		1070	Support vector machine	0.49	NA	-34.74%	-0.26
		1071	Random forest	0.49	NA	-35.16%	-0.26
	6	24	Convolutional neural networks	0.73	NA		
		1078	Support vector machine	0.64	NA	-12.57%	-0.09
		1079	Random forest	0.66	NA	-9.71%	-0.07
	7	23	Convolutional neural networks	0.70	NA		
		1074	Support vector machine	0.63	NA	-10.32%	-0.07
		1075	Random forest	0.65	NA	-6.98%	-0.05
	8	19	Convolutional neural networks	0.84	NA		
		1068	Support vector machine	0.63	NA	-25.72%	-0.22
		1069	Random forest	0.59	NA	-29.79%	-0.25

This is a non-peer-reviewed preprint submitted to EarthArXiv.

Pub. ID	Gr. No.	Identif. ID	ML/DL models	Overall accuracy	F1-score	Relative difference (%)	Absolute difference
	9	20	Convolutional neural networks	0.77	NA		
		1072	Support vector machine	0.76	NA	-1.46%	-0.01
		1073	Random forest	0.56	NA	-27.55%	-0.21
	10	21	Convolutional neural networks	0.79	NA		
		1076	Support vector machine	0.68	NA	-14.26%	-0.11
		1077	Random forest	0.66	NA	-16.58%	-0.13
10	11	33	Convolutional neural networks	0.92	NA		
		1080	Gradient boosting	0.84	NA	-9.29%	-0.09
		1081	Random forest	0.80	NA	-13.04%	-0.12
12	12	35	Convolutional neural networks	NA	0.95		
		1082	Support vector machine	NA	0.82	-13.89%	-0.13
		1083	Random forest	NA	0.81	-15.14%	-0.14
16	13	55	CNN-based attention	0.84	NA		
		1085	Support vector machine	0.66	NA	-21.45%	-0.18
		1086	Object based support vector machine	0.74	NA	-12.70%	-0.11
17	14	57	Convolutional neural networks	0.83	NA		
		1087	Random forest	0.44	NA	-46.67%	-0.39
		1088	Support vector machine	0.49	NA	-40.99%	-0.34
20	15	65	Convolutional neural networks	NA	0.80		
		1090	Random forest	NA	0.70	-12.50%	-0.10
	16	61	Convolutional neural networks	NA	0.80		
		1089	Random forest	NA	0.70	-12.50%	-0.10
	17	66	Convolutional neural networks	NA	0.80		
		1091	Random forest	NA	0.70	-12.50%	-0.10
24	18	110	Convolutional neural networks	NA	0.30		
		1095	Random forest	NA	0.55	83.33%	0.25
	19	111	Convolutional neural networks	NA	0.39		
		1096	Random forest	NA	0.61	56.41%	0.22
27	20	146	Convolutional neural networks	NA	0.93		
		1098	K-nearest neighbor	NA	0.65	-30.81%	-0.29
		1099	Random forest	NA	0.74	-20.79%	-0.19

This is a non-peer-reviewed preprint submitted to EarthArXiv.

Pub. ID	Gr. No.	Identif. ID	ML/DL models	Overall accuracy	F1-score	Relative difference (%)	Absolute difference
		1100	Support vector machine	NA	0.77	-17.19%	-0.16
	21	155	Convolutional neural networks	NA	0.97		
		1101	K-nearest neighbor	NA	0.89	-8.20%	-0.08
		1102	Random forest	NA	0.91	-5.54%	-0.05
		1103	Support vector machine	NA	0.93	-3.73%	-0.04
41	22	230	Convolutional neural networks	0.92	NA		
		1104	Decision tree	0.61	NA	-33.55%	-0.31
		1105	Random forest	0.67	NA	-27.45%	-0.25
44	23	241	Convolutional neural networks	NA	0.96		
		1106	Support vector machine	NA	0.86	-10.91%	-0.11
	24	242	Convolutional neural networks	NA	0.90	-6.34%	-0.06
		1107	Support vector machine	NA	0.70	-27.23%	-0.26
47	25	257	Convolutional neural networks	0.97	NA		
		1108	Support vector machine	0.91	NA	-5.88%	-0.06
		1109	Random forest	0.90	NA	-7.43%	-0.07
		1110	Maximum likelihood	0.87	NA	-4.54%	-0.04
65	26	348	Convolutional neural networks	0.81	NA		
		1111	Random forest	0.60	NA	-26.03%	-0.21
	27	351	Convolutional neural networks	0.94	NA		
		1112	Random forest	0.64	NA	-31.77%	-0.30
90	28	409	Convolutional neural networks	NA	0.87		
		1113	Support vector machine	NA	0.82	-5.75%	-0.05
91	29	417	Convolutional neural networks	1.00	NA		
		1115	Support vector machine	0.96	NA	-3.89%	-0.04
		1116	K-nearest neighbor	0.92	NA	-7.56%	-0.08
95	30	431	Convolutional neural networks	0.83	NA		
		1117	Random forest	0.52	NA	-37.27%	-0.31
		1118	Support vector machine	0.52	NA	-37.03%	-0.31
96	31	434	Convolutional neural networks	0.88	NA		
		1119	Random forest	0.83	NA	-5.57%	-0.05
		1120	Support vector machine	0.87	NA	-1.02%	-0.01

This is a non-peer-reviewed preprint submitted to EarthArXiv.

Pub. ID	Gr. No.	Identif. ID	ML/DL models	Overall accuracy	F1-score	Relative difference (%)	Absolute difference
98	32	459	Convolutional neural networks	0.85	NA		
		1121	Random forest	0.81	NA	-5.18%	-0.04
		1122	Support vector machine	0.84	NA	-1.30%	-0.01
134	33	624	Convolutional neural networks	0.98	NA		
		1123	Support vector machine	0.97	NA	-0.97%	-0.01
136	34	631	Convolutional neural networks	0.96	NA		
		1124	Support vector machine	0.65	NA	-32.32%	-0.31
		1125	Random forest	0.85	NA	-10.88%	-0.10
	35	643	Convolutional neural networks	0.93	NA		
		1128	Support vector machine	0.45	NA	-52.15%	-0.49
		1129	Random forest	0.73	NA	-21.57%	-0.20
	36	637	Convolutional neural networks	0.99	NA		
		1126	Support vector machine	0.68	NA	-30.97%	-0.31
		1127	Random forest	0.76	NA	-23.51%	-0.23
145	37	679	Convolutional neural networks	0.89	NA		
		1130	Random forest	0.66	NA	-26.16%	-0.23
		1131	Support vector machine	0.64	NA	-27.62%	-0.25
158	38	695	CNN-based attention	0.87	NA		
		1132	K-means	0.75	NA	-13.79%	-0.12
		1133	ISODATA	0.56	NA	-35.63%	-0.31
		1134	Random forest	0.81	NA	-6.90%	-0.06
		1135	Support vector machine	0.84	NA	-3.45%	-0.03
161	39	699	CNN-based attention	NA	0.75		
		1136	Random forest	NA	0.60	-20.58%	-0.16
	40	700	CNN-based attention	NA	0.77		
		1137	Random forest	NA	0.68	-11.51%	-0.09
195	41	782	CNN-based attention	NA	0.94		
		1138	Random forest	NA	0.85	-9.50%	-0.09
	42	783	CNN-based attention	NA	0.95		
		1139	Random forest	NA	0.86	-9.51%	-0.09
236	43	1016	Convolutional neural networks	NA	0.74		

Pub. ID	Gr. No.	Identif. ID	ML/DL models	Overall accuracy	F1-score	Relative difference (%)	Absolute difference
		1140	Random forest	NA	0.54	-27.03%	-0.20
		1143	CatBoost	NA	0.55	-25.68%	-0.19
	44	1017	Convolutional neural networks	NA	0.72		
		1141	Random forest	NA	0.66	-8.33%	-0.06
		1144	CatBoost	NA	0.79	9.72%	0.07
	45	1018	Convolutional neural networks	NA	0.74		
		1142	Random forest	NA	0.70	-5.41%	-0.04
		1145	CatBoost	NA	0.85	14.86%	0.11

Note: There were 28 reviewed publications conducting controlled comparisons between shallow machine learning and deep learning approaches, while two of them did not report explicit evaluation performance of shallow machine learning approaches, thus, they are not listed in this table (Publication ID = 43 and 64). However, they claimed literally that their deep learning approaches outperformed their shallow machine learning approaches.

This is a non-peer-reviewed preprint submitted to EarthArXiv.

Table S5. The protocol of extracted metadata.

Metadata types	No.	Metadata	Note
Basic information	1	Publication ID	
	2	Identification ID	
	3	Title	
	4	Authors	
	5	Journal	
	6	Year	
	7	DOI	
Tree species	8	Country	
	9	Biome	Boreal, temperate, subtropical, tropical, or arid
	10	Species	Scientific name
	11	Genus	Scientific name
	12	Number of Classes	
	13	Sample imbalance	The ratio of the largest to the smallest class sample size.
Remote sensing data	14	Data type	2D, 2D + 3D, Other
	15	Data input	
	16	Sensor platform	UAV, crewed aircraft, satellite etc.
	17	Resolution	Spatial resolution (cm)
	18	Multi-temporal data	Yes or No
Deep learning model	19	Computer vision task	
	20	Model family	
	21	Deep learning framework	
	22	F1-score	
	23	Overall accuracy	
	24	IoU	
	25	Average accuracy	
	26	Kappa	
	27	Precision	
	28	Recall	

Table S6. The full list of publications and all extracted data used in the meta-analysis

See attached supplementary Excel file "*Supplementary_Database_Review.xlsx*"

This is a non-peer-reviewed preprint submitted to EarthArXiv.

Table S7. List of identified species and their frequencies per biome.

No.	Species	Frequency	No.	Species	Frequency
	Boreal			Arid	
1	*Picea abies*	4	1	*Juniperus ashei*	1
2	*Pinus sylvestris*	4	2	*Phoenix dactylifera*	1
3	*Betula pendula*	2	3	*Prosopis glandulosa*	1
4	*Picea glauca*	2	4	*Quercus virginiana*	1
5	*Pinus contorta*	2			
6	*Abies holophylla*	1			
7	*Pinus koraiensis*	1			
8	*Populus tremula*	1			
	Temperate			Temperate	
1	*Acer rubrum*	8	92	*Cerasus nipponica*	1
2	*Betula pendula*	7	93	*Cercidiphyllum japonicum*	1
3	*Fagus sylvatica*	7	94	*Chamaecyparis lawsoniana*	1
4	*Ginkgo biloba*	7	95	*Chengiopanax sciadophylloides*	1
5	*Pinus sylvestris*	7	96	*Chusquea quila*	1
6	*Abies alba*	6	97	*Cinnamomum camphora*	1
7	*Picea abies*	6	98	*Cornus kousa*	1
8	*Pinus ponderosa*	6	99	*Crataegus laevigata*	1
9	*Pseudotsuga menziesii*	6	100	*Crataegus monogyna*	1
10	*Sophora japonica*	6	101	*Crataegus phaenopyrum*	1
11	*Betula platyphylla*	5	102	*Crataegus pinnatifida*	1
12	*Juglans mandshurica*	5	103	*Drimys winteri*	1
13	*Pinus strobus*	5	104	*Eucalyptus camaldulensis*	1
14	*Acer saccharum*	4	105	*Eucalyptus globulus*	1
15	*Fraxinus mandshurica*	4	106	*Eucalyptus pulchella*	1
16	*Pinus koraiensis*	4	107	*Eucalyptus robusta*	1
17	*Pinus tabuliformis*	4	108	*Eucalyptus viminalis*	1
18	*Quercus rubra*	4	109	*Eucryphia cordifolia*	1
19	*Tsuga canadensis*	4	110	*Fagus crenata*	1
20	*Abies balsamea*	3	111	*Fallopia japonica*	1
21	*Abies concolor*	3	112	*Ficus altissima*	1

This is a non-peer-reviewed preprint submitted to EarthArXiv.

No.	Species	Frequency	No.	Species	Frequency
	Temperate			Temperate	
22	*Acer pensylvanicum*	3	113	*Ficus microcarpa*	1
23	*Acer pseudoplatanus*	3	114	*Fitzroya cupressoides*	1
24	*Acer tataricum*	3	115	*Fraxinus angustifolia*	1
25	*Calocedrus decurrens*	3	116	*Gevuina avellana*	1
26	*Carpinus betulus*	3	117	*Gleditsia triacanthos*	1
27	*Fagus grandifolia*	3	118	*Glyptostrobus pensilis*	1
28	*Fraxinus chinensis*	3	119	*Gordonia lasianthus*	1
29	*Pinus lambertiana*	3	120	*Haloxylon ammodendron*	1
30	*Pinus resinosa*	3	121	*Ilex crenata*	1
31	*Populus nigra*	3	122	*Juglans cinerea*	1
32	*Quercus alba*	3	123	*Juglans nigra*	1
33	*Robinia pseudoacacia*	3	124	*Juniperus chinensis*	1
34	*Salix matsudana*	3	125	*Juniperus virginiana*	1
35	*Thuja occidentalis*	3	126	*Koelreuteria bipinnata*	1
36	*Ulmus pumila*	3	127	*Koelreuteria paniculata*	1
37	*Acacia mearnsii*	2	128	*Larix decidua*	1
38	*Acer platanoides*	2	129	*Larix olgensis*	1
39	*Aesculus hippocastanum*	2	130	*Laurelia sempervirens*	1
40	*Ailanthus altissima*	2	131	*Laureliopsis philippiana*	1
41	*Alnus glutinosa*	2	132	*Liquidambar styraciflua*	1
42	*Amygdalus davidiana*	2	133	*Lomatia hirsuta*	1
43	*Betula alleghaniensis*	2	134	*Luma apiculata*	1
44	*Betula papyrifera*	2	135	*Lyonia lucida*	1
45	*Callitris rhomboidea*	2	136	*Malus domestica*	1
46	*Carya glabra*	2	137	*Malus micromalus*	1
47	*Fraxinus excelsior*	2	138	*Nothofagus alessandri*	1
48	*Fraxinus pennsylvanica*	2	139	*Nothofagus alpina*	1
49	*Juglans regia*	2	140	*Nothofagus dombeyi*	1
50	*Larix gmelinii*	2	141	*Nothofagus obliqua*	1
51	*Larix laricina*	2	142	*Nyssa biflora*	1
52	*Liriodendron tulipifera*	2	143	*Nyssa sylvatica*	1

This is a non-peer-reviewed preprint submitted to EarthArXiv.

No.	Species	Frequency	No.	Species	Frequency
	Temperate			Temperate	
53	*Melaleuca pustulata*	2	144	*Persea lingue*	1
54	*Phellodendron amurense*	2	145	*Picea asperata*	1
55	*Pinus armandii*	2	146	*Picea glauca*	1
56	*Pinus palustris*	2	147	*Picea koraiensis*	1
57	*Pinus taeda*	2	148	*Pilgerodendron uviferum*	1
58	*Platanus acerifolia*	2	149	*Pinus banksiana*	1
59	*Platycladus orientalis*	2	150	*Pinus elliottii*	1
60	*Prunus armeniaca*	2	151	*Pinus nigra*	1
61	*Prunus avium*	2	152	*Pinus tabulaeformis*	1
62	*Prunus cerasifera*	2	153	*Platanus occidentalis*	1
63	*Prunus domestica*	2	154	*Podocarpus nubigenus*	1
64	*Prunus serotina*	2	155	*Populus deltoides*	1
65	*Pyrus calleryana*	2	156	*Populus tomentosa*	1
66	*Quercus coccinea*	2	157	*Prunus Kwanzan*	1
67	*Quercus laevis*	2	158	*Prunus blireiana*	1
68	*Sabina chinensis*	2	159	*Prunus serrulata*	1
69	*Sorbus aucuparia*	2	160	*Prunus subhirtella*	1
70	*Sorbus commixta*	2	161	*Punica granatum*	1
71	*Ulmus japonica*	2	162	*Quercus geminata*	1
72	*Abies fargesii*	1	163	*Quercus hemisphaerica*	1
73	*Abies mariesii*	1	164	*Quercus laurifolia*	1
74	*Acacia dealbata*	1	165	*Quercus liaotungensis*	1
75	*Acacia melanoxylon*	1	166	*Quercus montana*	1
76	*Acer griseum*	1	167	*Quercus nigra*	1
77	*Acer macrophyllum*	1	168	*Quercus palustris*	1
78	*Acer mono*	1	169	*Quercus petraea*	1
79	*Acer palmatum*	1	170	*Quercus robur*	1
80	*Acer saccharinum*	1	171	*Quercus variabilis*	1
81	*Acer truncatum*	1	172	*Salix babylonica*	1
82	*Acer tschonoskii*	1	173	*Sequoia sempervirens*	1
83	*Amelanchier grandiflora*	1	174	*Sequoiadendron giganteum*	1

This is a non-peer-reviewed preprint submitted to EarthArXiv.

No.	Species	Frequency	No.	Species	Frequency
	Temperate			Temperate	
84	*Amelanchier laevis*	1	175	*Styrax japonicus*	1
85	*Amomyrtus luma*	1	176	*Taxodium distichum*	1
86	*Amomyrtus meli*	1	177	*Taxus cuspidata*	1
87	*Caldcluvia paniculata*	1	178	*Thuja plicata*	1
88	*Carya tomentosa*	1	179	*Tilia cordata*	1
89	*Castanea dentata*	1	180	*Tilia europaea*	1
90	*Castanea sativa*	1	181	*Tilia platyphyllos*	1
91	*Castanopsis hystrix*	1			
	Tropical			Tropical	
1	*Licania tomentosa*	4	22	*Cedrela odorata*	1
2	*Pachira aquatica*	4	23	*Cocos nucifera*	1
3	*Terminalia catappa*	4	24	*Couratari macrosperma*	1
4	*Caesalpinia pluviosa*	3	25	*Elaeis guineensis*	1
5	*Senna siamea*	3	26	*Euterpe precatoria*	1
6	*Tamarindus indica*	3	27	*Ficus microcarpa*	1
7	*Bertholletia excelsa*	2	28	*Handroanthus serratifolius*	1
8	*Delonix regia*	2	29	*Hevea brasiliensis*	1
9	*Dipteryx alata*	2	30	*Hymenaea courbaril*	1
10	*Mauritia flexuosa*	2	31	*Hymenaea parvifolia*	1
11	*Acacia mearnsii*	1	32	*Iriartea deltoidea*	1
12	*Anacardium occidentale*	1	33	*Laguncularia racemosa*	1
13	*Apuleia leiocarpa*	1	34	*Melia azedarach*	1
14	*Areca catechu*	1	35	*Neltuma pallida*	1
15	*Artocarpus heterophyllus*	1	36	*Phyllocarpus riedelii*	1
16	*Attalea butyracea*	1	37	*Plumeria rubra*	1
17	*Avicennia schaueriana*	1	38	*Pouteria coriacea*	1
18	*Azadirachta indica*	1	39	*Rhizophora mangle*	1
19	*Bauhinia acreana*	1	40	*Sclerolobium melanocarpu*	1
20	*Cecropia hololeuca*	1	41	*Syagrus romanzoffiana*	1
21	*Cecropia juranyiana*	1			

This is a non-peer-reviewed preprint submitted to EarthArXiv.

No.	Species	Frequency	No.	Species	Frequency
	Subtropical			Subtropical	
1	*Cunninghamia lanceolata*	10	101	*Celtis sinensis*	1
2	*Pinus massoniana*	7	102	*Cercidiphyllum japonicum*	1
3	*Cinnamomum camphora*	6	103	*Chengiopanax sciadophylloides*	1
4	*Pinus elliottii*	6	104	*Cinnamodendron dinisii*	1
5	*Carya cathayensis*	5	105	*Cinnamomum verum*	1
6	*Delonix regia*	5	106	*Cryptomeria fortunei*	1
7	*Eucalyptus urophylla*	5	107	*Cryptomeria japonica*	1
8	*Ginkgo biloba*	5	108	*Cupania vernalis*	1
9	*Metasequoia glyptostroboides*	5	109	*Cyclobalanopsis glauca*	1
10	*Cedrus deodara*	4	110	*Erythrina falcata*	1
11	*Ficus microcarpa*	4	111	*Eucalyptus citriodora*	1
12	*Illicium verum*	4	112	*Eucalyptus globulus*	1
13	*Koelreuteria paniculata*	4	113	*Evodiopanax innovans*	1
14	*Salix babylonica*	4	114	*Fagus crenata*	1
15	*Abies concolor*	3	115	*Fagus japonica*	1
16	*Abies magnifica*	3	116	*Fraxinus chinensis*	1
17	*Calocedrus decurrens*	3	117	*Fraxinus lanuginosa*	1
18	*Camphora officinarum*	3	118	*Ginkgo Biloba*	1
19	*Castanopsis hystrix*	3	119	*Glyptostrobus pensilis*	1
20	*Dimocarpus longan*	3	120	*Hibiscus tiliaceus*	1
21	*Eucalyptus grandis*	3	121	*Hovenia dulcis*	1
22	*Magnolia grandiflora*	3	122	*Hovenia tomentella*	1
23	*Pinus contorta*	3	123	*Ilex chinensis*	1
24	*Pinus jeffreyi*	3	124	*Ilex latifolia*	1
25	*Pinus lambertiana*	3	125	*Ilex macropoda*	1
26	*Platanus acerifolia*	3	126	*Ilex micrococca*	1
27	*Quercus kelloggii*	3	127	*Ilex pedunculosa*	1
28	*Sapindus mukorossi*	3	128	*Kalopanax septemlobus*	1
29	*Acacia dealbata*	2	129	*Kandelia obovata*	1
30	*Acacia melanoxylon*	2	130	*Lagerstroemia indica*	1
31	*Acer palmatum*	2	131	*Liquidambar formosana*	1

This is a non-peer-reviewed preprint submitted to EarthArXiv.

No.	Species	Frequency	No.	Species	Frequency
	Subtropical			Subtropical	
32	*Acer rubrum*	2	132	*Litchi chinensis*	1
33	*Aegiceras corniculatum*	2	133	*Livistona chinensis*	1
34	*Alstonia scholaris*	2	134	*Lyonia ovalifolia*	1
35	*Araucaria angustifolia*	2	135	*Magnolia obovata*	1
36	*Camellia oleifera*	2	136	*Magnolia salicifolia*	1
37	*Campomanesia xanthocarpa*	2	137	*Malus tschonoskii*	1
38	*Carica papaya*	2	138	*Mangifera indica*	1
39	*Cedrela fissilis*	2	139	*Manglietia glauca*	1
40	*Chamaecyparis obtusa*	2	140	*Mango indica*	1
41	*Chorisia speciosa*	2	141	*Matayba elaeagnoides*	1
42	*Dicranopteris dichotoma*	2	142	*Meliosma myriantha*	1
43	*Eucalyptus robusta*	2	143	*Michelia chapensis*	1
44	*Liquidambar styraciflua*	2	144	*Michelia macclurei*	1
45	*Lithraea brasiliensis*	2	145	*Michelia odora*	1
46	*Luehea divaricata*	2	146	*Mimosa scabrella*	1
47	*Musa nana*	2	147	*Miscanthus sinensis*	1
48	*Nectandra megapotamica*	2	148	*Morella rubra*	1
49	*Osmanthus fragrans*	2	149	*Mosla chinensis*	1
50	*Pinus palustris*	2	150	*Mytilaria laosensis*	1
51	*Pinus taeda*	2	151	*Nyssa sylvatica*	1
52	*Podocarpus lambertii*	2	152	*Ostrya japonica*	1
53	*Quercus geminata*	2	153	*Phoenix sylvestris*	1
54	*Quercus laevis*	2	154	*Photinia serrulata*	1
55	*Quercus nigra*	2	155	*Phyllostachys edulis*	1
56	*Rhizophora stylosa*	2	156	*Phyllostachys heterocycla*	1
57	*Schinus terebinthifolia*	2	157	*Phyllostachys pubescens*	1
58	*Zelkova serrata*	2	158	*Pinus clausa*	1
59	*Abies firma*	1	159	*Pinus densiflora*	1
60	*Acacia confusa*	1	160	*Pinus hwangshanensis*	1
61	*Acer buergerianum*	1	161	*Pinus strobus*	1
62	*Acer carpinifolium*	1	162	*Pinus taiwanensis*	1

This is a non-peer-reviewed preprint submitted to EarthArXiv.

No.	Species	Frequency	No.	Species	Frequency
	Subtropical			Subtropical	
63	*Acer cinnamomifolium*	1	163	*Pinus yunnanensis*	1
64	*Acer forrestii*	1	164	*Platanus orientalis*	1
65	*Acer mono*	1	165	*Populus davidiana*	1
66	*Acer negundo*	1	166	*Populus simonii*	1
67	*Acer nipponicum*	1	167	*Populus tremula*	1
68	*Acer sieboldianum*	1	168	*Prunus cerasifera*	1
69	*Adenanthera pavonina*	1	169	*Prunus grayana*	1
70	*Aesculus turbinata*	1	170	*Prunus jamasakura*	1
71	*Albizia julibrissin*	1	171	*Pseudolarix amabilis*	1
72	*Alnus nepalensis*	1	172	*Psychotria serpens*	1
73	*Amygdalus persica*	1	173	*Pterocarya rhoifolia*	1
74	*Araucaria cunninghamii*	1	174	*Pterocarya stenoptera*	1
75	*Archontophoenix alexandrae*	1	175	*Pyrus sorotina*	1
76	*Aria alnifolia*	1	176	*Quercus acuta*	1
77	*Aria japonica*	1	177	*Quercus aliena*	1
78	*Armeniaca mume*	1	178	*Quercus crispula*	1
79	*Artocarpus nitidus*	1	179	*Quercus glauca*	1
80	*Averrhoa carambola*	1	180	*Quercus hemisphaerica*	1
81	*Avicennia marina*	1	181	*Quercus salicina*	1
82	*Bauhinia purpurea*	1	182	*Quercus serrata*	1
83	*Betula alnoides*	1	183	*Quercus virginiana*	1
84	*Betura grossa*	1	184	*Robinia pseudoacacia*	1
85	*Bischofia javanica*	1	185	*Sabina chinensis*	1
86	*Blechnum orientale*	1	186	*Sago palm*	1
87	*Bruguiera gymnorrhiza*	1	187	*Schinus lentiscifolius*	1
88	*Camellia sinensis*	1	188	*Sebastiania commersoniana*	1
89	*Camptotheaca acuminata*	1	189	*Sonneratia apetala*	1
90	*Carmona microphylla*	1	190	*Sophora japonica*	1
91	*Carpinus cordata*	1	191	*Stewartia monadelpha*	1
92	*Carpinus japonica*	1	192	*Symplocos prunifolia*	1
93	*Carpinus laxiflora*	1	193	*Taxodium ascendens*	1

This is a non-peer-reviewed preprint submitted to EarthArXiv.

No.	Species	Frequency	No.	Species	Frequency
	Subtropical			Subtropical	
94	*Carpinus tschonoskii*	1	194	*Terminalia mantaly*	1
95	*Carya dabieshanensis*	1	195	*Ternstroemia gymnanthera*	1
96	*Carya glabra*	1	196	*Tsuga sieboldii*	1
97	*Carya illinoinensis*	1	197	*Ulmus pumila*	1
98	*Castanea crenata*	1	198	*Wodyetia bifurcata*	1
99	*Castanopsis cuspidata*	1	199	*Ziziphus lotus*	1
100	*Catalpa speciosa*	1			

Table S8. The ten most frequently studied tree species and their per-class F1-score across studies, ranked by Median F1-score (high to low).

Species	Min.	Max.	Mean	Median	St.d	N
Pinus sylvestris	0.2400	0.9900	0.8165	0.9000	0.1846	56
Picea abies	0.6950	0.9655	0.8608	0.8746	0.0876	50
Delonix regia	0.7338	0.9254	0.8442	0.8630	0.0607	11
Ginkgo biloba	0.4202	1.0000	0.8293	0.8581	0.1505	59
Cunninghamia lanceolata	0.1041	0.9778	0.7976	0.8235	0.1412	51
Cinnamomum camphora	0.2800	0.9900	0.7180	0.7128	0.1971	23
Abies alba	0.3400	0.8700	0.6634	0.6700	0.1327	41
Fagus sylvatica	0.1480	0.9000	0.6688	0.6650	0.1842	40
Betula pendula	0.0700	0.9909	0.6478	0.6202	0.2520	45
Acer rubrum	0.1514	0.9613	0.4787	0.4650	0.2442	8

"St.d", standard deviation; "N", number of identifications.